Author(s): Al-Rasheed, Hessa H.; Al-Majid, Abdullah Mohammed; Ali, M.; Haukka, Matti; Ramadan, Sherif; Soliman, Saied M.; El-Faham, Ayman; Domingo, Luis R.; Barakat, Assem

Title: [3 + 2] Cycloadditions in Asymmetric Synthesis of Spirooxindole Hybrids Linked to Triazole and Ferrocene Units : X-ray Crystal Structure and MEDT Study of the Reaction Mechanism

Year: 2022

Version: Published version

Please cite the original version:

Al-Rasheed, H. H., Al-Majid, A. M., Ali, M., Haukka, M., Ramadan, S., Soliman, S. M., El-Faham, A., Domingo, L. R., & Barakat, A. (2022). [3 + 2] Cycloadditions in Asymmetric Synthesis of Spirooxindole Hybrids Linked to Triazole and Ferrocene Units : X-ray Crystal Structure and MEDT Study of the Reaction Mechanism. Symmetry, 14(10), Article 2071. https://doi.org/10.3390/sym14102071

symmetry

MDPI

Article

[3 + 2] Cycloadditions in Asymmetric Synthesis of Spirooxindole Hybrids Linked to Triazole and Ferrocene Units: X-ray Crystal Structure and MEDT Study of the Reaction Mechanism

Hessa H. Al-Rasheed [1], Abdullah Mohammed Al-Majid [1], M. Ali [1], Matti Haukka [2], Sherif Ramadan [3], Saied M. Soliman [4], Ayman El-Faham [4], Luis R. Domingo [5] and Assem Barakat [1,*]

[1] Department of Chemistry, College of Science, King Saud University, P.O. Box 2455, Riyadh 11451, Saudi Arabia
[2] Department of Chemistry, University of Jyväskylä, P.O. Box 35, FI-40014 Jyväskylä, Finland
[3] Chemistry Department, Michigan State University, East Lansing, MI 48824, USA
[4] Department of Chemistry, Faculty of Science, Alexandria University, P.O. Box 426, Alexandria 21321, Egypt
[5] Department of Organic Chemistry, University of Valencia, 46100 Valencia, Spain
* Correspondence: ambarakat@ksu.edu.sa; Tel.: +966-11467-5992 or +966-11467-5901

Abstract: Derivatization of spirooxindole having triazole and ferrocene units was achieved by the [3 + 2] cycloaddition (32CA) reaction approach. Reacting the respective azomethine ylide (AY) intermediate generated in situ with the ethylene derivative produced novel asymmetric cycloadducts with four contiguous asymmetric carbons in an overall high chemical yield with excellent regioselectivity and diastereoselectivity. X-Ray single-crystal structure analyses revealed, with no doubt, the success of the synthesis of the target compounds. The 32CA reaction of AY **5b** with ferrocene ethylene **1** has been studied within MEDT. This 32CA reaction proceeds via a *two-stage one-step* mechanism involving a high asynchronous transition state structure, resulting from the nucleophilic attack of AY **5b** on the β-conjugated position of ferrocene ethylene **1**. The supernucleophilic character of AY **5b** and the strong electrophilic character of ferrocene ethylene **1** account for the high polar character of this 32CA reaction. Further, Hirshfeld analyses were used to describe the molecular packing of compounds **4b, 4e, 4h** and **4i**.

Keywords: asymmetric synthesis; spirooxindole; triazole; ferrocene; azomethine ylide; [3 + 2] cycloaddition reaction; MEDT study

Citation: Al-Rasheed, H.H.; Al-Majid, A.M.; Ali, M.; Haukka, M.; Ramadan, S.; Soliman, S.M.; El-Faham, A.; Domingo, L.R.; Barakat, A. [3 + 2] Cycloadditions in Asymmetric Synthesis of Spirooxindole Hybrids Linked to Triazole and Ferrocene Units: X-ray Crystal Structure and MEDT Study of the Reaction Mechanism. *Symmetry* **2022**, *14*, 2071. https://doi.org/10.3390/sym14102071

Academic Editors: Mingyou Hu and Le Liu

Received: 7 September 2022
Accepted: 2 October 2022
Published: 5 October 2022

1. Introduction

The arena of diversity-oriented and combinatorial organic synthesis to construct heterocyclic hybrids with structurally diverse and pharmacologically importance has received a lot of attention in the last decades. The utilization of a simple starting material that is commercially available with the concepts of atom economy and environmental aspects is a pronounced challenge and attractive research for the chemical industry as well as the scientific community [1].

Spirohybrid heterocycles have received great attention from researchers, including chemists as well as medicinal/pharmaceutical researchers, due to their diverse importance for the applications of these hybrids in different fields.

The preferred synthetic approach to construct symmetric and asymmetrical spirohybrids is the multi-component reaction (MCRs) approach, which enables researchers to construct interesting and highly divergent spirohybrid heterocycles in a one-pot process with multiple bonds, with the advantage of having fewer workup steps, facile mechanization, simple purification and extraction, tractability and reproducibility and thus makes this approach more eco-friendly and follows atom economy [2,3]. Specifically, spiropyrrolidine

heterocycles exist in many synthetic and natural compounds, which possess many pharmacological interesting properties and can be synthesized by [3 + 2] cycloaddition (32CA) based on multi-component reactions (MCRs) [4]. Many natural alkaloids embody this spiropyrrolidine structural motif, such as horsfiline arediscovered, as a native medicine [5]. Further, spirotryprostatine A and B [6] and mitraphylline have been reported as high-efficacy anti-cancer agents [7]. Apart from naturally occurring compounds, a huge number of synthetic spiropyrrolidines analogs have been designed, synthesized and evaluated against different targets, including cancer activity [8,9], local anesthetics [10], analgesic and anti-inflammation [11] and other activity, such as anti-mycobacterial [12] and anti-microbial agents [13], and others [14–20].

Indeed, the ferrocene motif is another interesting organometallic scaffold owing to its potential pharmaceutical properties, photochemical and thermal stability, as well as synthetic versatility [21,22]. Notably, organic compounds engrafted with ferrocene scaffold exhibit many biological activities, such as anti-microbial, antimalarial and anti-cancer activities [23]. Interestingly, hydroxyferrocifen and ferroquine, which are ferrocene-based compounds, have already been employed in clinical trials for breast cancer treatment and as an antimalarial drug candidates, respectively [24,25]. The hybridization of the spiropyrrolidine with the ferrocene organometallic scaffold could provide an interesting lead organic molecule for further research.

The 1,2,3-Triazole unit is also another interesting pharmacophore that has received a lot of attention in the area of synthetic chemistry due to its interesting pharmacological applications [26] such as carbonic anhydrase inhibitors [27], tuberculosis treatment [28,29] and an antimalarial agent [30]. The combination of a triazole with the ferrocene organometallic scaffold has received a lot of interest from researchers due to the wide range of applications of these hybrid compounds in different disciplines, including medicinal chemistry as biosensing probes, biochemistry, conducting polymer chemistry, materials science and supramolecular chemistry [31–38]. To construct highly functionalized spirohybrid heterocycles having a combined triazole with the ferrocene organometallic scaffold is a challenge.

Based on these findings, and in continuation of our research program [39,40], which focuses on multi-component reactions for accessing highly divergent, functionalized molecules having different pharmacophores, such as spiropyrrolidine, 1,2,3-triazole unit and ferrocene organometallic scaffold in a single compound, might be a lead of paramount interest in drug discovery. We reported here the synthesis, characterizations and X-ray structure analysis of a new set of spiropyrrolidine analogs, along with the mechanistic insights for the 32CA reaction approach (Figure 1).

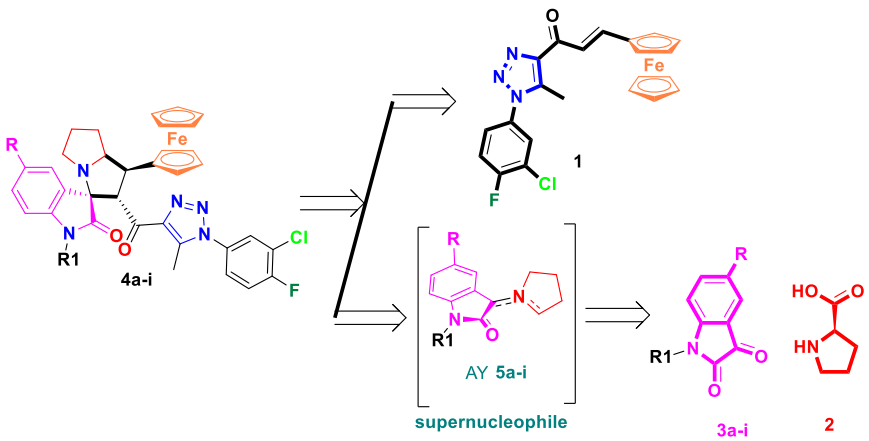

Figure 1. Retrosynthetic analysis for the spirooxindole/triazole/ferrocene-based pharmacophores.

2. Materials and Methods

The chemical utilized and instrumentations for the study investigation are provided in the Supplementary Materials. The synthesis of ethylene derivative **1** was prepared according to the method reported in the literature [40].

*2.1. Synthesis of Spirooxindole Hybrids **4a-i***

Isatin derivatives **3a-i** (0.35 mmol) and L-proline **2** (0.35 mmol) were mixed with ethylene derivative **1** (0.35 mmol) in a one-pot reaction in 10 mL MeOH, which was refluxed for 5 h using an oil bath system. The reaction was monitored by TLC (EtOAc: n-Hexane, 3:7). Subsequently, the reaction mixture was allowed to cool at RT overnight, and after slow evaporation, reddish-brown crystalline compounds suitable for physico-chemical analysis, including single-crystal X-ray diffraction analysis, were obtained.

2.1.1. (2′S,3R)-2′-(1-(3-Chloro-4-fluorophenyl)-5-methyl-1H-1,2,3-triazole-4-carbonyl)- 1′-(ferrocin-2-yl)-1′,2′,5′,6′,7′,7a′-hexahydrospiro[indoline-3,3′-pyrrolizin]-2-one **4a**

Yield: 92%; ^{1}H NMR (400 MHz, DMSO-d_6) δ 10.19 (s, 1H, NH), 7.83 (t, *J* = 4.4 Hz, 1H, Ar-H), 7.72 (t, *J* = 8.9 Hz, 1H, Ar-H), 7.52–7.43 (m, 2H, Ar-H), 7.09–6.97 (m, 1H, Ar-H), 6.81 (t, *J* = 7.5 Hz, 1H, Ar-H), 6.57 (d, *J* = 7.7 Hz, 1H, Ar-H), 5.14 (d, *J* = 10.8 Hz, 1H, CHCO), 4.26 (s, 5H, Cp-H), 4.18–4.08 (m, 4H, Cp-H), 4.02 (q, *J* = 7.1 Hz, 1H, NCH), 3.82 (s, 1H, NCHCH), 3.46 (t, *J* = 10.1 Hz, 1H, NCH_2), 2.75 (q, *J* = 7.6, 7.2 Hz, 1H, NCH_2), 2.15 (d, *J* = 9.5 Hz, 1H, CH_2), 2.07 (s, 3H, CH_3), 1.92 (m, 1H, CH_2), 1.81–1.72 (m, 2H, CH_2); ^{13}C NMR (101 MHz, DMSO-d_6) δ 194.01, 180.03, 170.94, 159.82, 157.33, 143.51, 143.06, 138.58, 132.21, 129.51, 125.91, 121.50, 121.31, 118.79, 109.67, 90.03, 72.36, 70.21, 68.95, 68.80, 67.55, 60.34, 55.50, 48.07, 27.20, 9.60; LC/MS (ESI, *m*/*z*): found 650.2 $[M + H]^+$, exact mass 649.13 for Chemical Formula: $C_{34}H_{29}ClFFeN_5O_2$. [Anal. Calcd. for $C_{34}H_{29}ClFFeN_5O_2$: C, 62.83; H, 4.50; N, 10.78; Found: C, 62.86; H, 4.52; N, 10.81].

2.1.2. (2′S,3R)-2′-(1-(3-Chloro-4-fluorophenyl)-5-methyl-1H-1,2,3-triazole-4-carbonyl)-5-methoxy-)- 1′-(ferrocin-2-yl)-1′,2′,5′,6′,7′,7a′-hexahydrospiro[indoline-3,3′-pyrrolizin]-2-one **4b**

Yield: 90%; ^{1}H NMR (400 MHz, DMSO-d_6) δ 10.19 (s, 1H, NH), 7.79 (s, 1H, Ar-H), 7.69 (t, J = 4.4 Hz, 1H, Ar-H), 7.46 (m, 1H, Ar-H), 7.14 (m, 1H, Ar-H), 7.03 (s, 1H, Ar-H), 6.90 (m, 1H, Ar-H), 6.73 (m, 1H, Ar-H), 5.09 (d, J = 10.8 Hz, 1H, CHCO), 4.29 (s, 5H, Cp-H), 4.13 (m, 4H, Cp-H), 2.95 (m, 2H, NHC_2), 2.74 (m, 1H, NCH_2), 2.34 (m, 1H, CH_2), 2.19 (s, 3H, CH_3), 2.02 (s, 3H, CH_3), 1.93 (m, 1H, CH_2), 1.79 (m, 2H, CH_2);^{13}C NMR (126 MHz, DMSO-d_6) δ 193.29, 178.57, 159.56, 158.03, 144.23, 143.19, 138.52, 132.06, 129.60, 128.09, 127.33, 126.97, 126.90, 125.17, 121.76, 121.47, 121.32, 118.84, 118.66, 108.43, 90.05, 71.97, 70.24, 68.91, 67.61, 67.57, 67.46, 67.42, 47.96, 43.16, 30.97, 27.46, 26.59, 9.46; LC/MS (ESI, *m*/*z*): found 680.28 $[M + H]^+$, exact mass 679.14 for Chemical Formula: $C_{35}H_{31}Cl_2FFeN_5O_2$. [Anal. Calcd. for $C_{35}H_{31}Cl_2FFeN_5O_2$: C, 61.83; H, 4.60; N, 10.30; Found: C, 61.89; H, 4.65; N, 10.27].

2.1.3. (2′S,3R)-2′-(1-(3-Chloro-4-fluorophenyl)-5-methyl-1H-1,2,3-triazole-4-carbonyl)-5-chloro-)-1′-(ferrocin-2-yl)-1′,2′,5′,6′,7′,7a′-hexahydrospiro[indoline-3,3′-pyrrolizin]-2-one **4c**

Yield: 91%; ^{1}H NMR (400 MHz, DMSO-d_6) δ 10.35 (s, 1H, NH), 7.78 (dt, J = 6.2, 2.9 Hz, 1H, Ar-H), 7.71–7.61 (m, 1H, Ar-H), 7.46 (ddd, J = 8.8, 4.2, 2.2 Hz, 1H, Ar-H), 7.11–7.03 (m, 1H, Ar-H),), 6.97 (d, J = 2.3 Hz, 1H, Ar-H), 6.57 (d, J = 8.1 Hz, 1H, Ar-H), 5.14 (d, J = 10.5 Hz, 1H, CHCO), 4.23 (s, 5H, Cp-H), 4.15–4.03 (m, 4H, Cp-H), 3.80 (s, 1H, NCH_2), 2.75–2.66 (m, 1H, NCH_2), 2.44–2.34 (m, 1H, CH_2), 2.15 (s, 3H, CH_3), 1.96 (d, J = 10.1 Hz, 1H, CH_2), 1.79 (m, 2H, CH_2); ^{13}C NMR (101 MHz, DMSO-d_6) δ 193.70, 179.69, 160.59, 158.19, 143.36, 142.03, 138.60, 130.18, 129.15, 128.85, 128.01, 126.63, 125.31, 121.69, 119.47, 111.89, 110.20, 89.71, 79.85, 79.52, 79.19, 72.05, 70.89, 69.76, 69.49, 68.56, 68.50, 68.44, 68.19, 68.12, 68.05, 67.99, 67.92, 67.31, 66.77, 65.99, 10.10, 8.87; LC/MS (ESI, *m*/*z*): found 684.21 $[M + H]^+$, exact mass 683.10 for Chemical Formula: $C_{34}H_{28}Cl_2FFeN_5O_2$. [Anal. Calcd. for $C_{34}H_{28}Cl_2FFeN_5O_2$: C, 59.67; H, 4.12; N, 10.23; Found: C, 59.65; H, 4.09; N, 10.25].

2.1.4. (2′S,3R)-2′-(1-(3-Chloro-4-fluorophenyl)-5-methyl-1H-1,2,3-triazole-4-carbonyl)-5-bromo-)- 1′-(ferrocin-2-yl)-1′,2′,5′,6′,7′,7a′-hexahydrospiro[indoline-3,3′-pyrrolizin]-2-one **4d**

Yield: 88%; ^{1}H NMR (400 MHz, DMSO-d_6) δ 10.39 (s, 1H, NH), 7.79 (dd, *J* = 6.3, 2.6 Hz, 1H, Ar-H), 7.69 (td, *J* = 8.8, 2.1 Hz, 1H, Ar-H), 7.50–7.41 (m, 1H, Ar-H), 7.22 (dd, *J* = 8.1, 2.1 Hz, 1H, Ar-H), 7.09 (s, 1H, Ar-H), 6.54 (d, *J* = 8.1 Hz, 1H, Ar-H), 5.14 (d, *J* = 10.4 Hz, 1H, CHCO), 4.24 (s, 5H, Cp-H), 4.17–4.06 (m, 4H, Cp-H), 3.81 (d, *J* = 2.1 Hz, 1H, NCH_2), 3.46 (t, *J* = 10.2 Hz, 1H, NCH_2), 2.74 (m, 1H, CH_2), 2.41 (m, 1H, CH_2), 2.17 (m, 2H, CH_2), 2.15 (s, 3H, CH_3), 1.96 (m, 1H, CH_2), 1.80 (s, 2H); ^{13}C NMR (101 MHz, DMSO-d_6) δ 183.06, 163.95, 159.61, 155.74, 143.34, 142.48, 138.73, 131.18, 130.95, 125.42, 121.78, 120.60, 119.74, 115.70, 115.55, 112.94, 112.49, 107.65, 107.02, 90.99, 79.86, 79.53, 79.20, 71.96, 68.21, 68.13, 68.06, 67.99, 45.19, 8.97; LC/MS (ESI, *m*/*z*): found 728.12 $[M + H]^+$, exact mass 727.04 for Chemical Formula: $C_{34}H_{28}BrClFFeN_5O_2$. [Anal. Calcd. for $C_{34}H_{28}BrClFFeN_5O_2$: C, 56.03; H, 3.87; N, 9.61; Found: C, 56.05; H, 3.88; N, 9.60].

2.1.5. (2′S,3R)-2′-(1-(3-Chloro-4-fluorophenyl)-5-methyl-1H-1,2,3-triazole-4-carbonyl)-5-fluoro-)- 1′-(ferrocin-2-yl)-1′,2′,5′,6′,7′,7a′-hexahydrospiro[indoline-3,3′-pyrrolizin]-2-one **4e**

Yield: 93%; ^{1}H NMR (400 MHz, DMSO-d_6) δ 10.21 (s, 1H, NH), 7.88 (dd, *J* = 6.5, 2.5 Hz, 1H, Ar-H), 7.72 (t, *J* = 8.9 Hz, 1H, Ar-H), 7.53 (dt, *J* = 6.2, 2.5 Hz, 1H, Ar-H), 6.97–6.85 (m, 2H, Ar-H), 6.57 (dd, *J* = 8.5, 4.5 Hz, 1H, Ar-H), 5.17 (d, *J* = 10.9 Hz, 1H, CHCO), 4.26 (s, 5H, Cp-H), 4.18–4.06 (m, 4H, Cp-H), 3.80 (s, 1H), 3.48 (d, *J* = 10.2 Hz, 1H, NCH_2), 2.50 (s, 1H), 2.37 (d, *J* = 8.9 Hz, 1H, NCH_2), 2.14 (s, 3H, CH_3), 1.98 (m, 1H, CH_2), 1.95 (m, 1H, CH_2), 1.80 (m, 2H, CH_2); ^{13}C NMR (101 MHz, DMSO-d_6) δ 193.74, 179.96, 161.34, 157.00, 143.38, 139.28, 138.72, 138.65, 132.25, 129.10, 127.66, 121.53, 120.15, 117.76, 116.22, 110.97, 89.82, 72.56, 70.77, 68.54, 68.21, 68.14, 68.06, 67.99, 67.27, 66.80, 66.48, 65.92, 57.27, 55.48, 10.08, 8.82; LC/MS (ESI, *m*/*z*): found 668.18 $[M + H]^+$, exact mass 667.12 for Chemical Formula: $C_{34}H_{28}ClF_2FeN_5O_2$. [Anal. Calcd. for $C_{34}H_{28}ClF_2FeN_5O_2$: C, 61.14; H, 4.23; N, 10.; Found: C, 61.19; H, 4.26; N, 10.53].

2.1.6. (2′S,3R)-2′-(1-(3-Chloro-4-fluorophenyl)-5-methyl-1H-1,2,3-triazole-4-carbonyl)-5-nitro-)- 1′-(ferrocin-2-yl)-1′,2′,5′,6′,7′,7a′-hexahydrospiro[indoline-3,3′-pyrrolizin]-2-one **4f**

Yield: 87%; ^{1}H NMR (400 MHz, DMSO-d_6) δ 11.06 (s, 1H, NH), 8.06 (dd, *J* = 8.8, 2.7 Hz, 1H, Ar-H), 7.85 (dd, *J* = 6.5, 2.7 Hz, 1H, Ar-H), 7.80 (d, *J* = 2.4 Hz, 1H, Ar-H), 7.70 (t, *J* = 8.9 Hz, 1H, Ar-H), 7.50 (dd, *J* = 8.1, 4.2 Hz, 1H, Ar-H), 6.82 (d, *J* = 8.4 Hz, 1H, Ar-H), 5.19 (d, *J* = 10.5 Hz, 1H, CHCO), 4.19–4.09 (m, 5H, Cp-H), 3.82 (s, 4H, Cp-H), 3.52 (t, *J* = 10.1 Hz, 1H, NCH_2), 2.75 (q, *J* = 7.6 Hz, 1H, NCH_2), 2.22–2.14 (m, 1H, NCH_2), 2.14 (s, 3H, CH_3), 1.98 (s, 1H, CH_2), 1.96 (d, *J* = 8.9 Hz, 1H, CH_2), 1.82 (td, *J* = 14.9, 14.1, 7.3 Hz, 2H, CH_2); ^{13}C NMR (101 MHz, DMSO-d_6) δ 193.57, 180.44, 180.38, 161.66, 160.32, 149.63, 143.21, 141.86, 139.49, 139.13, 132.09, 129.07, 128.97, 127.94, 126.85, 126.24, 123.69, 123.51, 121.52, 121.33, 119.27, 118.15, 110.92, 88.70, 71.41, 68.65, 68.18, 68.10, 68.03, 66.96, 8.85; LC/MS (ESI, *m*/*z*): found 695.20 $[M + H]^+$, exact mass 694.12 for Chemical Formula: $C_{34}H_{28}ClFFeN_6O_4$. [Anal. Calcd. for $C_{34}H_{28}ClFFeN_6O_4$: C, 58.76; H, 4.06; N, 12.09; Found: C, 58.74; H, 4.08; N, 12.13].

2.1.7. (2′S,3R)-2′-(1-(3-Chloro-4-fluorophenyl)-5-methyl-1H-1,2,3-triazole-4-carbonyl)-6-chloro-)- 1′-(ferrocin-2-yl)-1′,2′,5′,6′,7′,7a′-hexahydrospiro[indoline-3,3′-pyrrolizin]-2-one **4g**

Yield: 89%; ^{1}H NMR (400 MHz, DMSO-d_6) δ 10.39 (s, 1H, NH), 7.81–7.66 (m, 1H, Ar-H), 7.55–7.46 (m, 1H, Ar-H), 7.00 (d, *J* = 8.1 Hz, 1H, Ar-H), 6.86 (dd, *J* = 8.1, 2.1 Hz, 1H, Ar-H), 6.59 (d, *J* = 1.9 Hz, 1H, Ar-H), 5.12 (d, *J* = 10.4 Hz, 1H, CHCO), 4.23 (s, 5H, Cp-H), 4.29–4.06 (m, 4H, Cp-H), 3.88–3.79 (m, 1H, NCH_2), 2.70 (dd, *J* = 16.9, 9.0 Hz, 1H, NCH_2), 2.39 (s, 1H, NCH_2), 2.16 (s, 3H, CH_3), 2.22–2.08 (m, 1H, CH_2), 1.96–1.90 (m, 1H, CH_2), 1.86–1.76 (m, 1H, CH_2); ^{13}C NMR (101 MHz, DMSO-d_6) δ 193.71, 179.92, 173.22, 166.58, 159.14, 158.34, 154.12, 144.63, 143.45, 138.69, 134.06, 132.44, 129.91, 129.19, 128.20, 126.52, 124.51, 121.61, 119.88, 113.01, 108.65, 93.89, 79.88, 79.55, 79.22, 71.91, 68.19, 68.12, 68.06,

67.99, 67.92, 67.06, 64.73, 10.17, 8.93; LC/MS (ESI, m/z): found 684.22 $[M + H]^+$, exact mass 683.10 for Chemical Formula: $C_{34}H_{28}Cl_2FFeN_5O_2$. [Anal. Calcd. for $C_{34}H_{28}Cl_2FFeN_5O_2$: C, 59.67; H, 4.12; N, 10.23; Found: C, 59.68; H, 4.10; N, 10.19].

2.1.8. (2′S,3R)-2′-(1-(3-Chloro-4-fluorophenyl)-5-methyl-1H-1,2,3-triazole-4-carbonyl)- 1-methyl-1′-(ferrocin-2-yl)-1′,2′,5′,6′,7′,7a′-hexahydrospiro[indoline-3,3′-pyrrolizin]-2-one **4h**

Yield: 85%; ^{1}H NMR (400 MHz, DMSO-d_6) δ 7.79 (s, 1H, Ar-H), 7.69 (s, 1H, Ar-H), 7.46 (s, 1H, Ar-H), 7.14 (s, 1H, Ar-H), 7.03 (s, 1H, Ar-H), 6.90 (s, 1H, Ar-H), 6.73 (s, 1H, Ar-H), 5.09 (s, 1H, CHCO), 4.29 (s, 5H, Cp-H), 4.13 (d, J = 20.2 Hz, 3H, Cp-H), 2.95 (s, 2H, NCH_2), 2.74 (s, 1H, CH_2), 2.34 (s, 3H, CH_3), 2.19 (s, 1H, CH_2), 2.02 (s, 3H, CH_3), 1.93 (s, 1H, CH_2), 1.79 (s, 2H, CH_2);^{13}C NMR (126 MHz, DMSO-d_6) δ 193.29, 178.57, 159.56, 158.03, 144.23, 143.19, 138.52, 132.06, 129.60, 128.09, 127.33, 126.97, 126.90, 125.17, 121.76, 121.47, 121.32, 118.84, 118.66, 108.43, 90.05, 71.97, 70.24, 68.91, 67.61, 67.57, 67.46, 67.42, 47.96, 43.16, 30.97, 27.46, 26.59, 9.46.; LC/MS (ESI, m/z): found 664.26 $[M + H]^+$, exact mass 663.15 for Chemical Formula: $C_{35}H_{31}Cl_2FFeN_5O_2$. [Anal. Calcd. for $C_{35}H_{31}Cl_2FFeN_5O_2$: C, 63.31; H, 4.71; N, 10.55; Found: C, 63.30; H, 4.70; N, 10.61].

2.1.9. (2′S,3R)-1-(2-Bromoethyl)-2′-(1-(3-chloro-4-fluorophenyl)-5-methyl-1H-1,2,3-triazole-4-carbonyl) -1′-(ferrocin-2-yl)-1′,2′,5′,6′,7′,7a′-hexahydrospiro[indoline-3,3′-pyrrolizin]-2-one **4i**

Yield: 86%; ^{1}H NMR (400 MHz, DMSO-d_6) δ 7.82 (d, J = 6.2 Hz, 1H, Ar-H), 7.70 (t, J = 8.9 Hz, 1H, Ar-H), 7.51 (s, 1H, Ar-H), 7.19–7.05 (m, 1H, Ar-H), 6.92 (d, J = 8.1 Hz, 1H, Ar-H), 5.16 (d, J = 10.9 Hz, 1H, CHCO), 4.29 (s, 5H, Cp-H), 4.09 (d, J = 5.8 Hz, 4H, Cp-H), 4.00 (d, J = 14.2 Hz, 1H, NCH_2), 3.87 (d, J = 17.4 Hz, 1H, NCH_2), 3.75 (s, 1H, CH_2), 3.56 (d, J = 16.6 Hz, 1H, CH_2), 3.49–3.38 (m, 1H, CH_2), 2.67 (d, J = 7.7 Hz, 1H, CH_2), 2.35 (s, 1H, CH_2), 2.24–2.17 (m, 1H, CH_2), 2.05 (s, 3H, CH_3), 1.93 (s, 1H, CH_2), 1.80 (s, 1H, CH_2); ^{13}C NMR (126 MHz, DMSO-d_6) δ 192.96, 178.57, 159.55, 157.56, 143.28, 142.95, 138.76, 132.07, 129.55, 128.15, 127.63, 127.00, 126.93, 125.06, 121.94, 121.43, 121.28, 118.76, 118.59, 109.06, 90.03, 71.84, 70.38, 68.94, 68.89, 67.60, 67.51, 67.28, 67.12, 47.51, 43.34, 40.66, 31.25, 29.63, 27.76, 9.54; Chemical Formula:. LC/MS (ESI, m/z): found 756.20 $[M + H]^+$, exact mass 755.08 for Chemical Formula: $C_{36}H_{34}BrClFFeN_5O_2$. [Anal. Calcd. for $C_{36}H_{34}BrClFFeN_5O_2$: C, 57.13; H, 4.26; N, 9.25; Found: C, 57.11; H, 4.28; N, 9.29].

2.2. Computational Details

The ωB97X-D functional [41], together with the standard 6-311G(d,p) basis set [42], was used in this molecular electron density theory (MEDT) study [43]. The transition state structures (TSs) were characterized by the presence of only one imaginary frequency. Solvent effects of methanol were taken into account by full optimization of the gas phase structures at the same computational level using the polarizable continuum model (PCM) [44,45]. Values of ωB97X-D/6-311G(d,p) enthalpies, entropies and Gibbs free energies in solution 1M [46] were calculated with standard statistical thermodynamics at 337.8 K [42] by PCM frequency calculations at the solvent-optimized structures. The global electron density transfer (GEDT) [47] values were computed by using the equation GEDT(f) = Σqf, where q is the natural charges [48,49] of the atoms belonging to one of the two frameworks (f) at the TS geometries. The conceptual density functional theory (CDFT) indices [50,51] were calculated by using the equations given in reference [51]. The Gaussian 16 suite of programs was used to perform the calculations [52].

2.3. X-ray Structure Determinations

The technical, experimental work and the software [53–59] for the single crystal X-ray diffraction analysis for the studied spirooxindole hybrids **4b, 4e, 4h** and **4i** are amended in the Supplementary Materials.

2.4. Hirshfeld Surface Analysis

The topology analyses were performed using Crystal Explorer 17.5 program [60].

3. Results and Discussion

3.1. Chemistry

The 32CA reaction approach employed for the synthesis of the target spirooxindole hybrids linked to the ferrocene and triazole units is depicted in Scheme 1 and follow our reported method [40]. The in situ azomethine ylide **5a-i** (AYs) was generated by reacting the isatin derivatives **3a-i** with the L-proline **2** and then, in a subsequent step, reacted with the dipolarphile ferrocene ethylene derivative **1** to construct the new spirooxindole pharmacologically interesting hybrids **4a-i**. The final cycloadducts target asymmetric molecules were provided in stereoselective fashion and a high-chemical yield. Four chiral centers were generated in the final compounds. The molecular structure's complexity of the synthesized spirooxindoles was deduced based on NMR spectroscopic analyses (Figures S3–S16; Supplementary Materials), which are found to be in full agreement with the proposed structures. Further, four successful crystalline compounds were obtained, and their structures were assigned unambiguously by single-crystal X-ray-diffraction analysis. The plausible mechanism confirms the regiospecific and the diastereospecifics of these kinds of spirooxindole analogs are followed based on the previously reported literature where the 32CA reaction pathway proceeds via *ortho*/*endo* in a *two-stage one-step* mechanism.

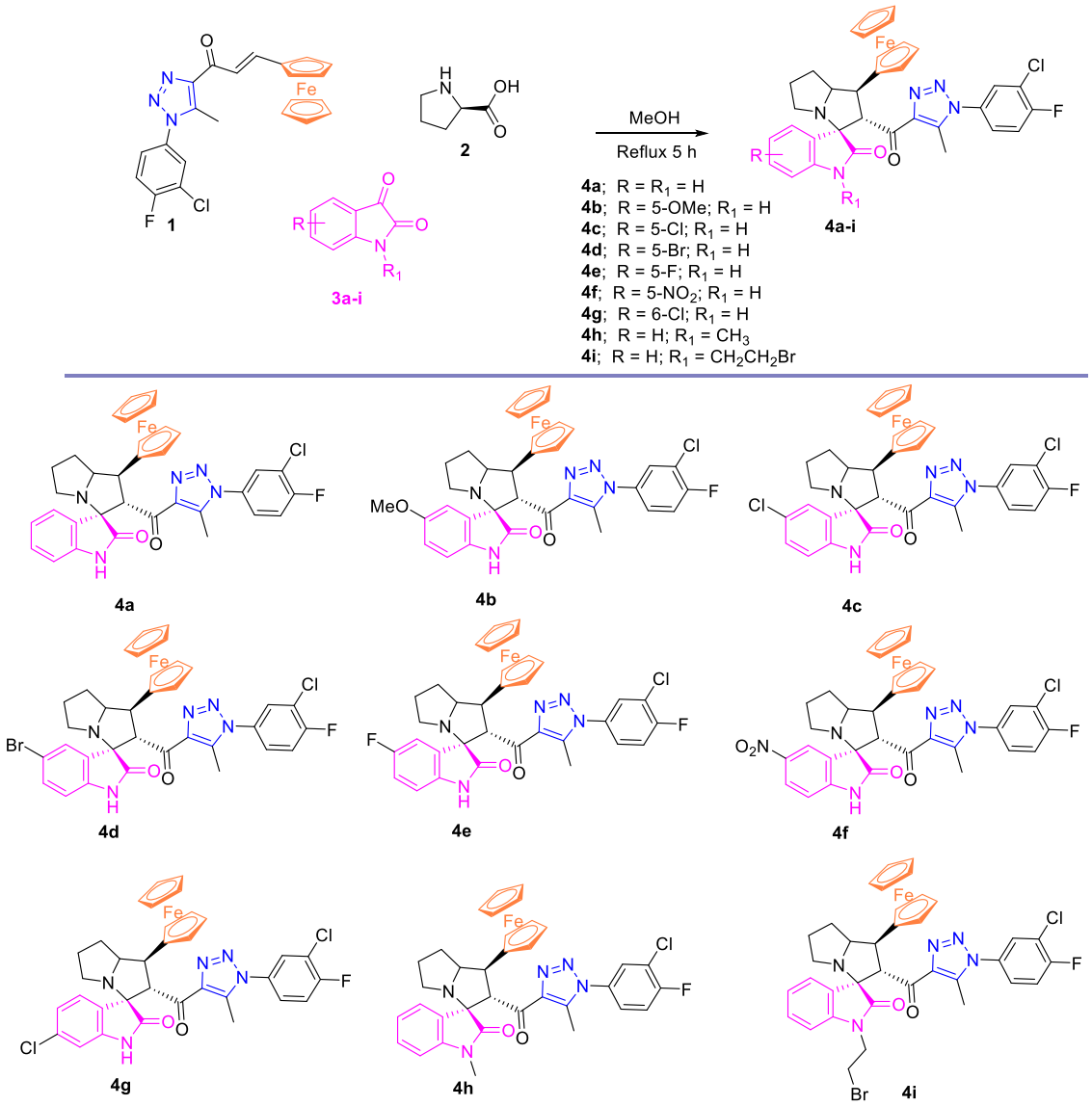

Scheme 1. Synthetic route for the new spirooxindole analogs **4a-i** engrafted with ferrocene and triazole nucleus.

3.2. Crystal-Structure Description of *4b*, *4e*, *4h* and *4i*

The X-ray structures of **4b, 4e, 4h** and **4i** confirmed with no doubt the success of the synthesis of the target compounds, as shown in Figure 2. All crystal data and refinement parameters are listed in Table 1.

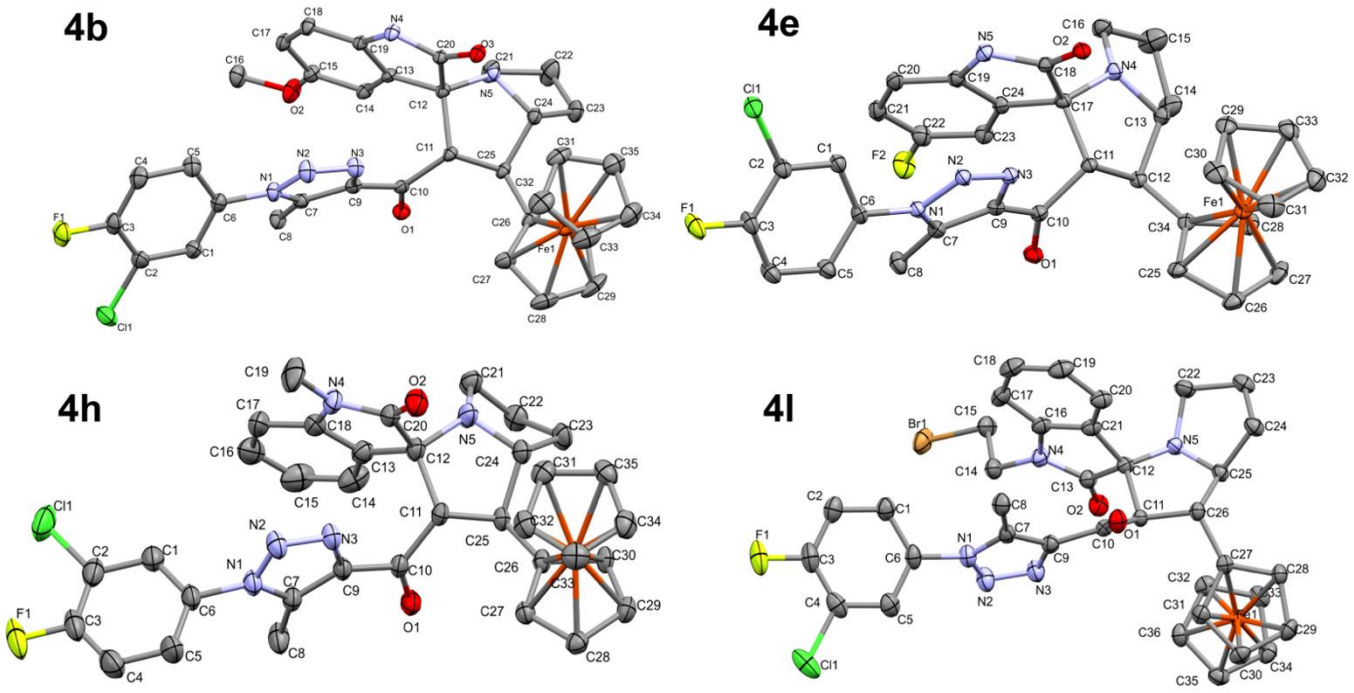

Figure 2. X-Ray structure of **4b, 4e, 4h** and **4i**. All hydrogen atoms were removed for better clarity. A summary of the most important distances is given in Table S1 (Supplementary Materials). For color codes: grey (carbon), red (oxygen), blue (nitrogen), green (chlorine), yellow (fluorine), brown (iron) and orange (bromine).

Table 1. Crystal data of **4b, 4e**, **4h** and **4i**.

	4b	**4e**	**4h**	**4i**
CCDC	2203019	2203020	2203021	2203022
empirical formula	$C_{36}H_{33}Cl_3FFeN_5O_3$	$C_{34}H_{28}ClF_2FeN_5O_2$	$C_{35}H_{31}ClFFeN_5O_2$	$C_{36}H_{32}BrClFFeN_5O_2$
fw	764.87	667.91	663.95	756.87
temp (K)	170(2)	120(2)	120(2)	120(2)
λ(Å)	0.71073	1.54184	1.54184	1.54184
cryst syst	Triclinic	Triclinic	Monoclinic	Monoclinic
space group	$P\bar{1}$	$P\bar{1}$	$P2_1/n$	$P2_1/c$
a (Å)	9.5779(2)	9.9037(2)	8.84939(4)	8.36150(10)
b (Å)	13.8939(3)	13.0148(3)	16.45070(9)	24.3249(2)
c (Å)	14.2414(3)	13.0497(2)	20.07254(9)	15.84530(10)
α(deg)	66.0890(10)	93.0000(10)	90	90
β (deg)	85.9040(10)	100.840(2)	91.7059(4)	95.8300(10)
γ(deg)	81.1600(10)	98.026(2)	90	90
V (Å^3)	1711.85(6)	1630.49(6)	2920.84(2)	3206.15(5)
Z	2	2	4	4
ρ_{calc} (Mg/m^3)	1.484	1.360	1.510	1.568
μ(Mo Kα) (mm^{-1})	0.725	4.880	5.393	6.396
No. reflns.	30,574	41,983	82,650	40,811
Unique reflns.	8128	6822	6154	6742
Completeness	99.4% [c]	99.9% [d]	100% [d]	100% [d]
GOOF (F^2)	1.026	1.070	1.042	1.041
R_{int}	0.0281	0.0426	0.0346	0.0340
R_1 [a] ($I \geq 2\sigma$)	0.0445	0.0411	0.0372	0.0363
wR_2 [b] ($I \geq 2\sigma$)	0.1005	0.1066	0.1052	0.0949

[a] $R_1 = \Sigma||F_o| - |F_c||/\Sigma|F_o|$. [b] $wR_2 = \{\Sigma[w(F_o^2 - F_c^2)^2]/\Sigma[w(F_o^2)^2]\}^{1/2}$. [c] θ = 25.242 and [d] θ = 33.92

Compound **4b** crystallizes in the triclinic crystal system and the *P-1* space group with Z = 2. The crystal parameters are presented in Table 1. Selected bond distances are given in Table S1 (Supplementary Materials). The asymmetric formula comprised one molecule of the target compound and one dichloromethane as the crystal solvent, which are connected with one another by weak C36-H36A···N5 and C36-H36A···O3 interactions. The hydrogen-acceptor distances are 3.546(3) and 3.215(3) Å, respectively (Figure 3).

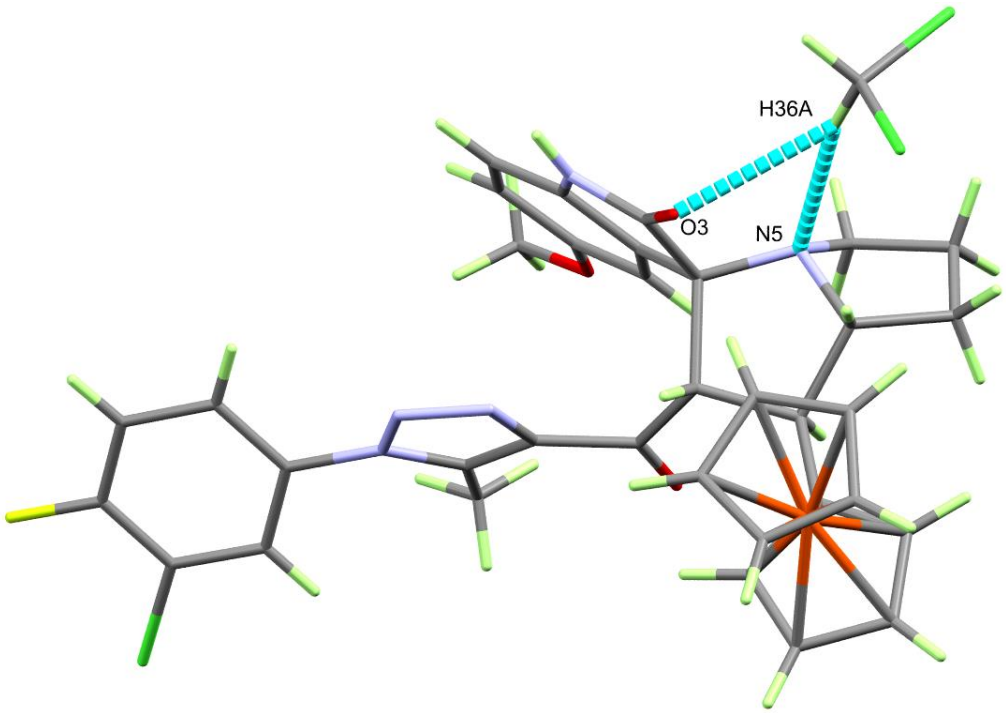

Figure 3. The C-H···N and C-H···O interactions between the target compound and the crystal solvent (CH_2Cl_2). For color codes: grey (carbon), red (oxygen), blue (nitrogen), green (chlorine), yellow (fluorine), brown (iron), light green (hydrogen).

Every two molecules of the target compound are connected by the classical N4-H4···O3 hydrogen bonding interaction. The hydrogen bond parameters are depicted in Table 2, while the hydrogen bond dimer is shown in Figure 4.

Table 2. Hydrogen bonds in 4b, 4h and 4i.

D-H···A	d(D-H)	d(H···A)	d(D···A)	<(DHA)	Symm. Codes
4b					
N(4)-H(4)···O(3)	0.84(3)	1.98(3)	2.821(2)	176(2)	1 −x + 2, −y, −z + 1
C(16)-H(16B)·····N(3)	0.980	2.547	3.513(3)	168.4	−1 + x, y, z
C(32)-H(32)·····O(2)	0.950	2.664	3.244(4)	119.89	−1 + x, y, z
C(8)-H(8A)·····O(1)	0.980	2.468	3.315(3)	144.44	1 − x, 1 − y, 1 − z
4h					
C4-H4···O2	0.95	2.44	3.373(3)	169	3/2 − x, −1/2 + y, 3/2 − z
C16-H16···F1	0.95	2.48	3.192(3)	131	1 − x, 1 − y, 2 − z
C19-H19C···O2	0.98	2.5	2.885(3)	103	
C25-H25···O1	1.00	2.47	2.831(2)	101	
C31-H31···O2	0.95	2.57	3.438(2)	152	
C33-H33···O1	0.95	2.6	3.541(2)	172	1 − x, 1 − y, 1 − z

Table 2. *Cont.*

D-H···A	d(D-H)	d(H···A)	d(D···A)	<(DHA)	Symm. Codes
4i					
C23-H23B···O2	0.99	2.58	3.403(3)	140	−1 + x, y, z
C26-H26···O1	1.00	2.41	2.816(3)	104	
C33-H33···Br1	0.95	2.93	3.759(3)	147	−1 + x, 3/2 − y, −1/2 + z
C34−H34···F1	0.95	2.46	3.207(3)	135	−1 + x, y, −1 + z

Additionally, the molecules of **4b** are further connected by weak nonclassical C-H···N and C-H···O interactions shown in the upper part of Figure S1 (Supplementary Materials) and listed in Table 2. The molecular packing schemes are shown in the lower part of Figure S1 (Supplementary Materials).

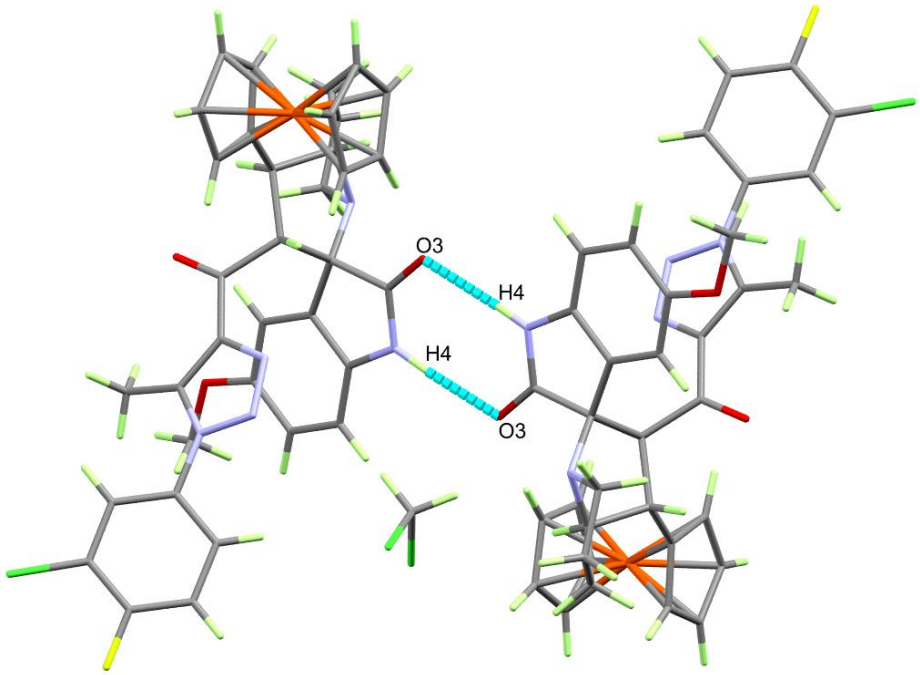

Figure 4. Centrosymmetric hydrogen-bonded dimer in **4b**. For color codes: grey (carbon), red (oxygen), blue (nitrogen), green (chlorine), yellow (fluorine), brown (iron) and light green (hydrogen).

The compounds **4h** and **4i** crystallize in the monoclinic crystal system with $Z = 4$. The unit cell parameters are depicted in Table 1. For these compounds, the packing is dominated by many weak interactions (Table 2). The presentation of these weak contacts found in **4h** and **4i** is shown in Figure 5. Since the structure of 4e comprised an indefinite amount of crystallized solvent, which was squeezed from the structure, the different intermolecular contacts the contributed to the molecular packing of this structure will not be described.

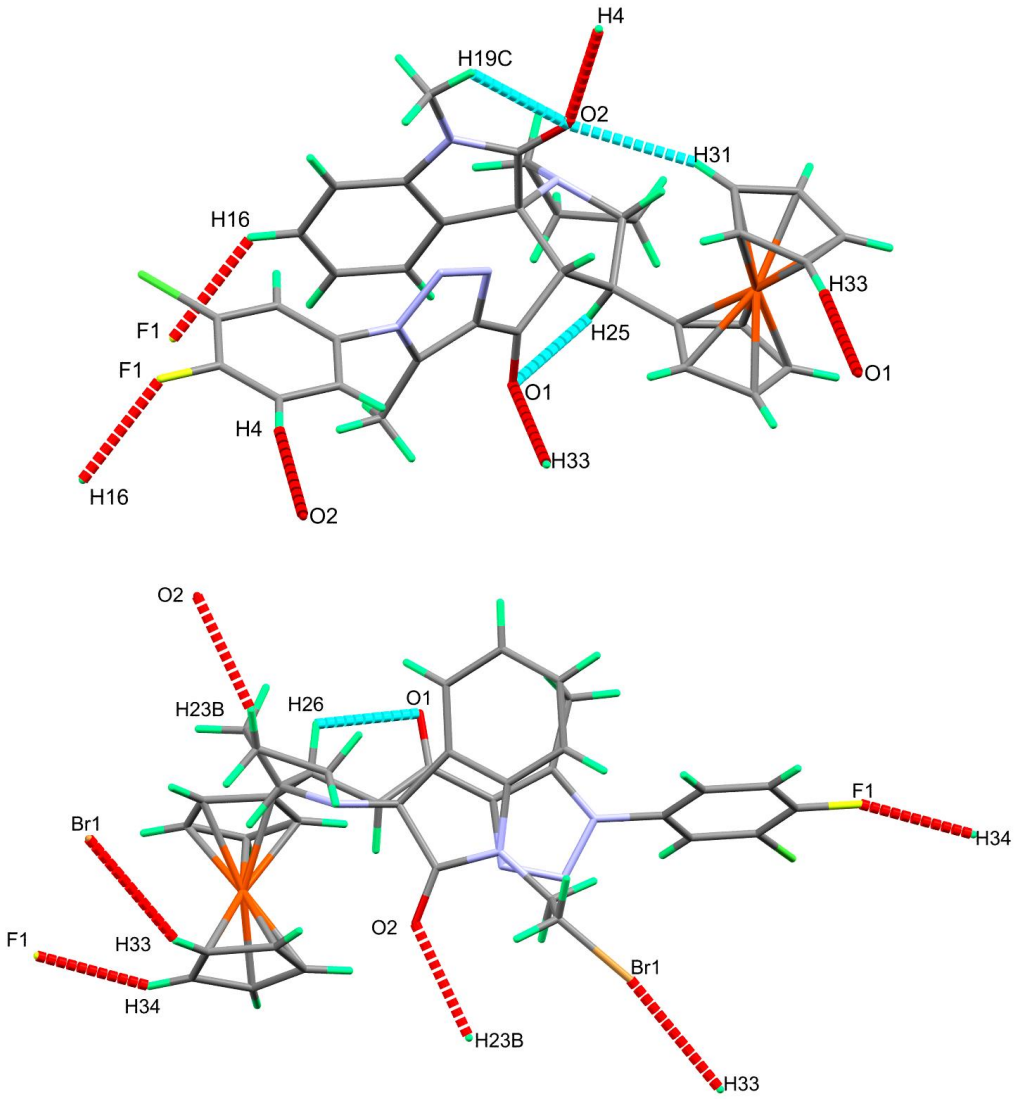

Figure 5. The most important interactions in the molecular packing of **4h** (**upper**) and **4i** (**lower**). For color codes: grey (carbon), red (oxygen), blue (nitrogen), yellow (fluorine), brown (iron), orange (bromine) and light green (hydrogen).

3.3. Hirshfeld Surface Analysis

In order to describe the different intermolecular contacts in the crystal structure of **4b** in detail, Hirshfeld calculations were performed. Different Hirshfeld surfaces are presented in Figure 6. The presence of a large number of red spots indicates regions in which there are important short-distance contacts. There are many O···H, N···H, C···H and H···H contacts occurring at shorter distances than the interacting atoms. The percentages of these contacts are 9.2%, 8.2%, 12.6% and 41.9%, respectively. Other contacts, such as Cl···H and F···H, contributed 15.1% and 5.7%, but they occurred at long interaction distances and hence are considered weak. Many contacts that also occurred at long interaction distances and contributed less to the molecular packing of **4b** are depicted in Figure 7.

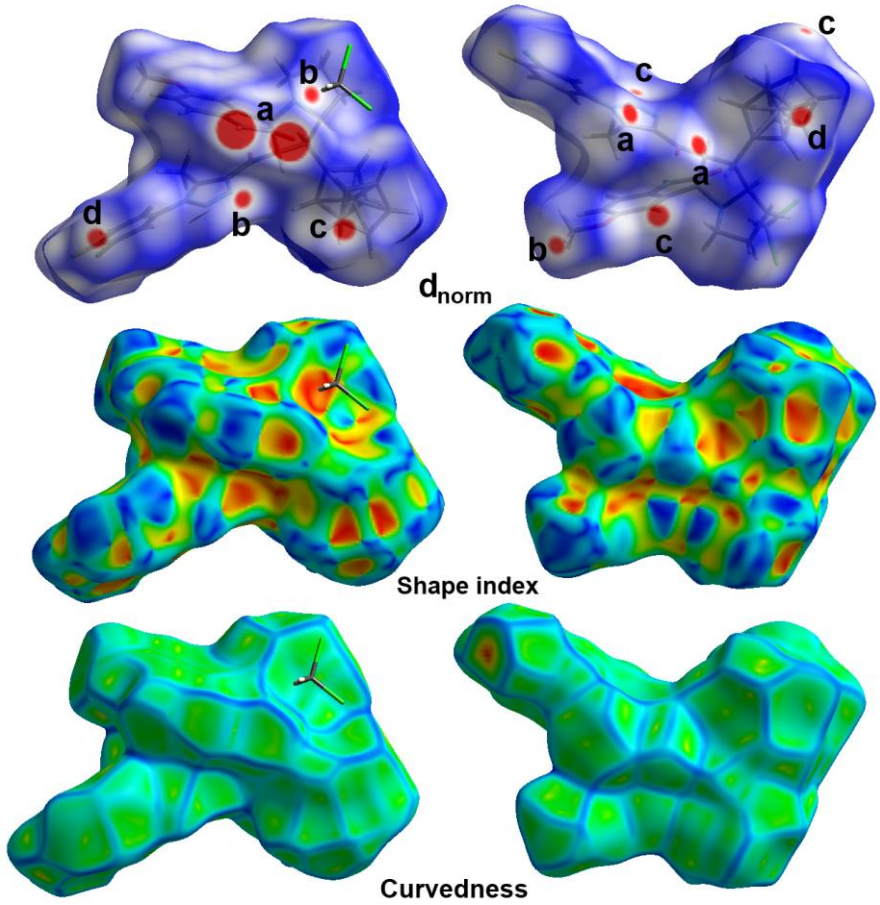

Figure 6. Hirshfeld surfaces of **4b**. The O· · · · · H (**a**), N· · · · · H (**b**), H· · · · · C (**c**) and H· · · · · H (**d**) appeared as red spots in d_{norm}.

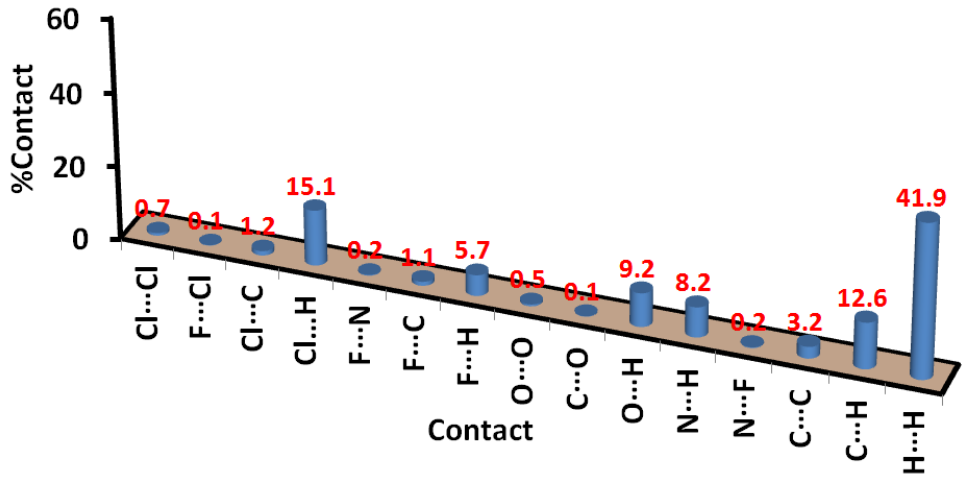

Figure 7. Intermolecular contacts and their percentages in **4b**.

Analysis of the fingerprint plots of the O· · · · · H, N· · · · · H, C· · · · · H and H· · · · · H contacts leave no doubt about the high percentages of the majority of these contacts and also that these interactions occur at short distances, as indicated from the sharp spikes corresponding to the O· · · · · H, N· · · · · H and C· · · · · H contacts (Figure 8). The O1· · · · · H8A (2.385 Å), O3· · · · · H4 (1.814 Å), O3· · · · · H36A (2.563 Å), N3· · · · · H16B (2.447 Å), C7· · · · · H33 (2.690 Å) and C32· · · · · H14 (2.525 Å) are the shortest intermolecular interactions that occurred in **4b**. In contrast, H4A· · · · · H29 (2.295 Å) is the shortest

H· · · · · H interaction, but it is slightly longer than the sum of the vdWs radii of two hydrogen atoms. Hence, the hydrogenic interactions are considered weak, long-distance contacts.

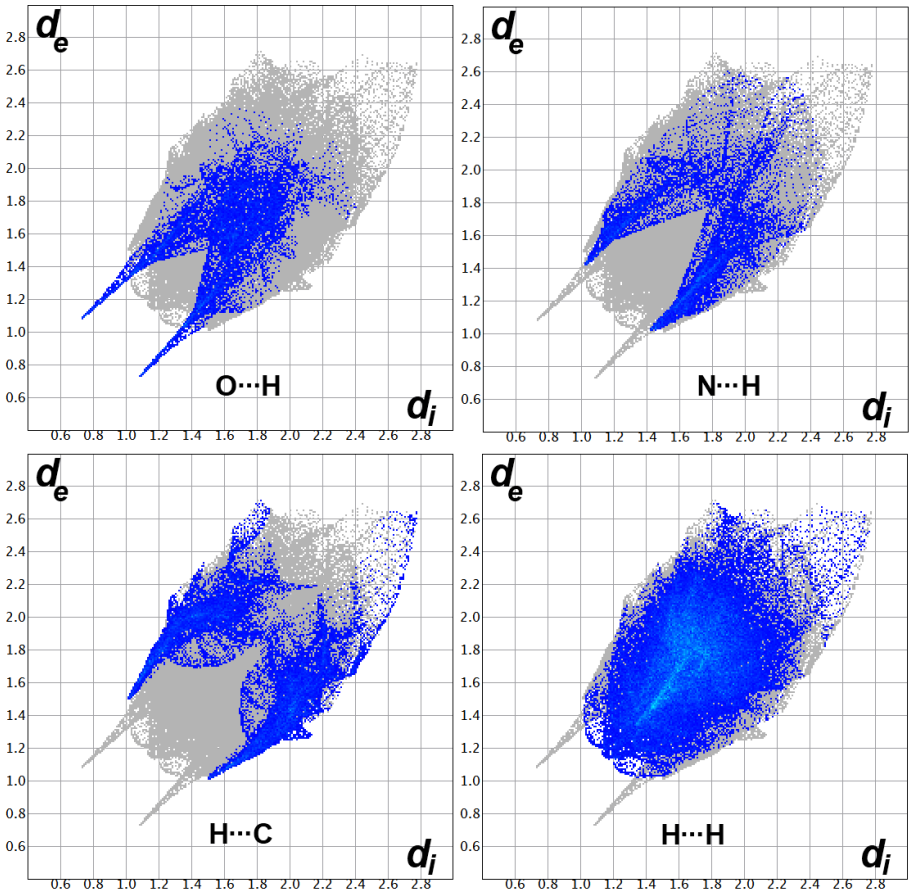

Figure 8. Decomposed fingerprint plots for short contacts in **4b**.

Interestingly, the careful inspection of the d_{norm} map revealed the presence of two red spots corresponding to the short C4· · · · · C2 (3.356 Å) contact. In the same region, there are red/blue triangle combinations in the shape index map. All these features revealed the importance of the π-π stacking interactions in the molecular packing of **4b** (Figure 9).

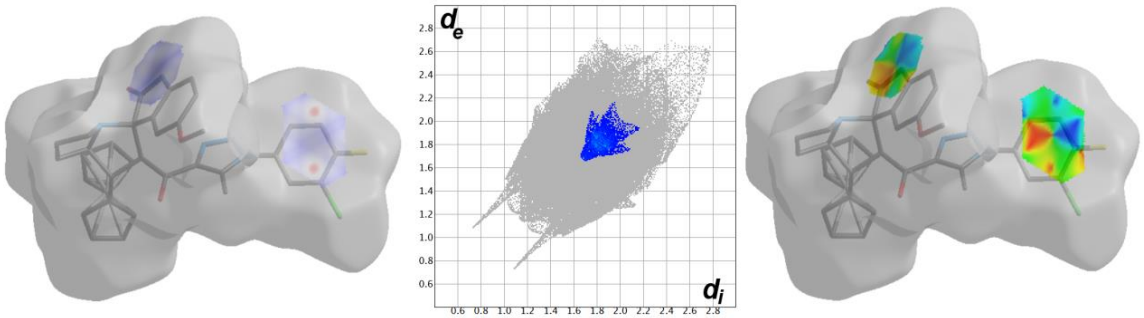

Figure 9. The d_{norm} (**left**), fingerprint plot (**middle**) and shape index (**right**) of π-π stacking interactions in **4b**.

The Hirshfeld analysis of **4h** sheds light on the significant intermolecular contacts in its crystal structure. Based on the present red spots in the d_{norm} map, the O· · · · · H, N· · · · · H, C· · · · · H and H· · · · · H contacts, as well as little contributions from the F· · · · · H and F· · · · · F interactions, are important in the molecular packing of **4h** (Figure 10). The distance of the F1· · · · · F1 interhalogen interaction is 2.713 Å and contributes only 0.7%

to the molecular packing. In addition, there are some Cl1· · · · · N5 (3.281 Å) contacts that contribute 0.5% of the whole contacts. The percentages of the other contacts are presented in Figure 11. It is clear that the major contacts are the H· · · · · H, C· · · · · H and Cl· · · · · H interactions.

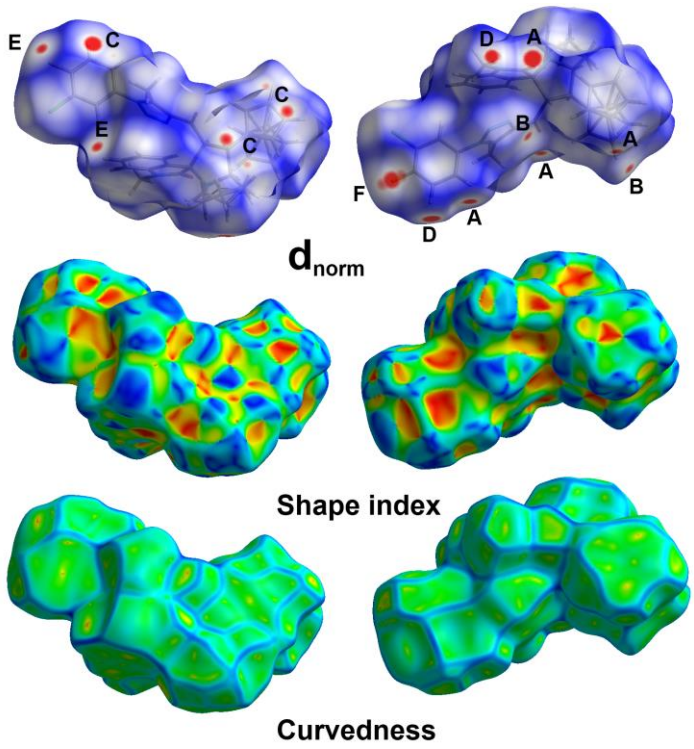

Figure 10. Hirshfeld surfaces of **4h**. O· · · · · H (**A**), N· · · · · H (**B**), H· · · · · C (**C**), H· · · · · H (**D**), F· · · · · H (**E**) and F· · · · · F (**F**) appeared as red spots in d_{norm}.

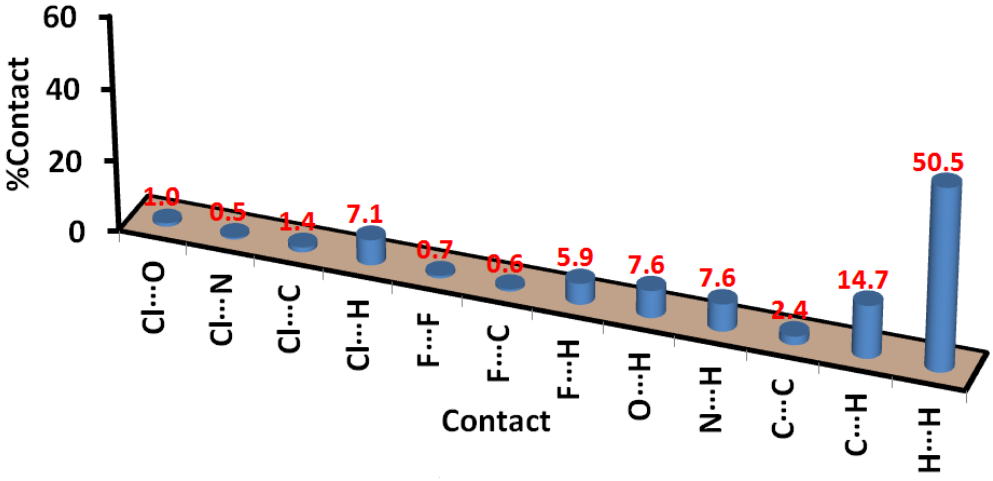

Figure 11. Intermolecular contacts and their percentages in **4h**.

The fingerprint plots of the most important contacts are shown in Figure 12, while a list of the short contacts is summarized in Table 3. As can be seen, there are short H· · · · · H, O· · · · · H, N· · · · · H, C· · · · · H, F· · · · · H, F· · · · · F and Cl· · · · · N contacts, as indicated by their appearance as sharp spikes in the fingerprint plots. Further, all the contacts presented in Table 3 are shorter than the vdWs radii sum of the interacting atoms.

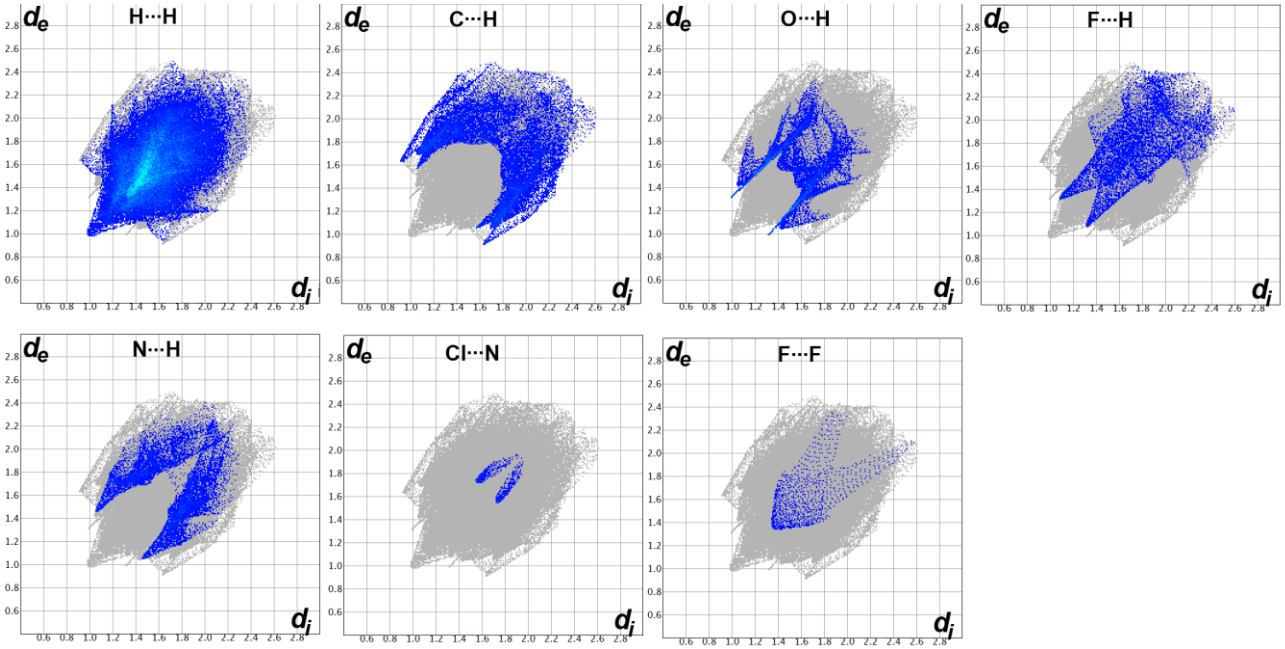

Figure 12. Decomposed fingerprint plots for short contacts in **4h**.

Table 3. The short contacts in **4h** and **4i**.

Contact	Distance	Contact	Distance
4h		**4i**	
H19C· · · · · H15	1.976	Br1· · · · · H28	2.927
C28· · · · · H23A	2.746	Br1· · · · · H33	2.82
C29· · · · · H25	2.631	F1· · · · · H34	2.371
C4· · · · · H22D	2.549	O2· · · · · H23B	2.513
C5· · · · · H21A	2.776	O1· · · · · H5	2.555
N3· · · · · H28	2.515	N2· · · · · H20	2.554
O2· · · · · H4	2.306	C32· · · · · H15B	2.579
O1· · · · · H33	2.466	C33· · · · · H15B	3.07
F1· · · · · H16	2.396	C34· · · · · H15B	2.78
Cl1· · · · · N5	3.281	C9· · · · · H8C	2.715
F1· · · · · F1	2.713		

In this case, the shortest π-π interaction occurred between C33 of the cyclopentadienyl moiety and the C17 atom, where the interaction distance is 3.432 Å, which is slightly longer than the vdWs radii sum of two carbon atoms. Hence, the π-π stacking interactions appeared as a white region in the d_{norm}. Further, the shape index revealed the presence of π-π stacking interactions where the percentage of the C· · · · · C contacts is 2.4% (Figure 13).

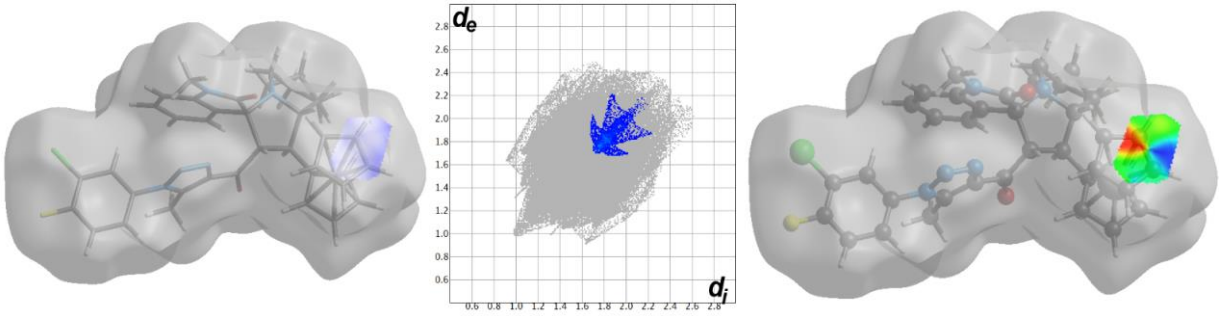

Figure 13. The d_{norm} (**left**), fingerprint plot (**middle**) and shape index (**right**) of π-π stacking interactions in **4h**.

For **4i**, the O· · · · · H, N· · · · · H, C· · · · · H, Br· · · · · H and F· · · · · H contacts are the most important in the molecular packing based on Hirshfeld analysis (Figure 14). Their percentages are 6.8%, 5.5%, 12.7%, 9.2% and 6.6%, respectively (Figure 15). The shortest O· · · · · H, N· · · · · H, C· · · · · H, Br· · · · · H and F· · · · · H contacts are listed in Table 3. All these interactions have the characteristic of short-distance interactions as these contacts appeared as red spots in the d_{norm} and sharp spikes in the fingerprint plot (Figure 16). Similar to **4i**, the π-π interactions occurred at longer distances than the vdWs radii sum of two carbon atoms. The shortest π-π interactions are C3· · · · · C29 and C2· · · · · C30 contacts, which also occurred between the cyclopentadienyl moiety and aromatic carbon atoms of the aryl group from an adjacent molecule (Figure S2, Supplementary Materials).

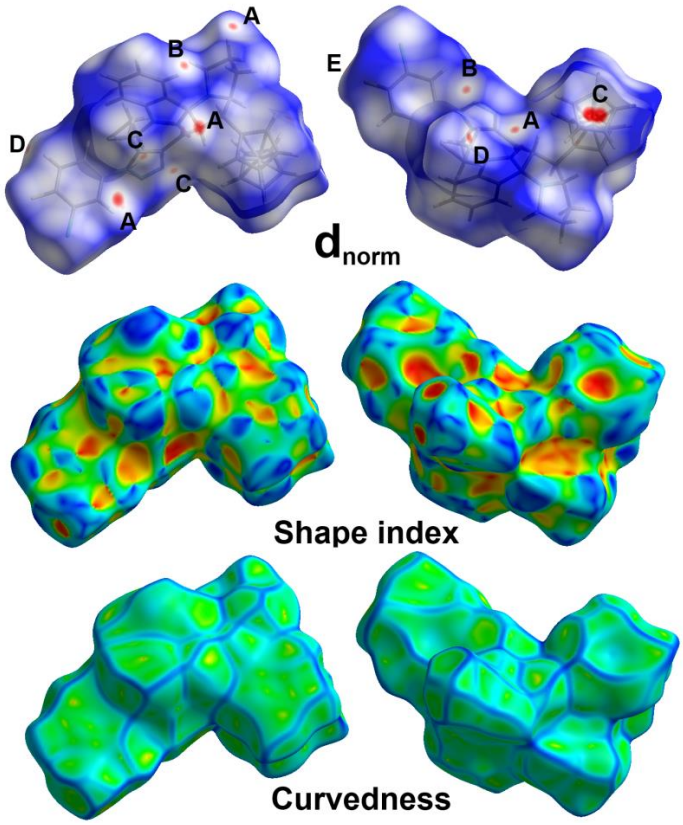

Figure 14. Hirshfeld surfaces of **4i**. The O· · · · · H (**A**), N· · · · · H (**B**), C· · · · · H (**C**), Br· · · · · H (**D**) and F· · · · · H (**E**) appeared as red spots in d_{norm}.

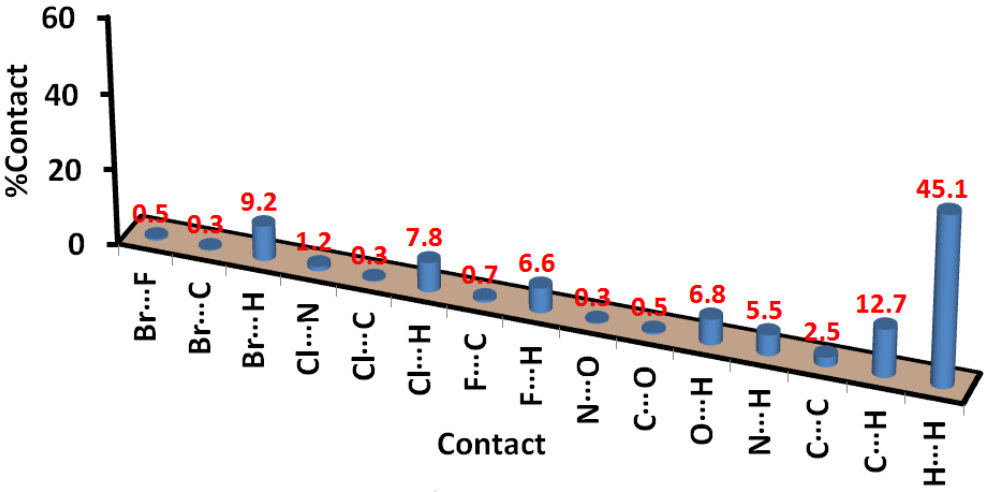

Figure 15. Intermolecular contacts and their percentages in **4i**.

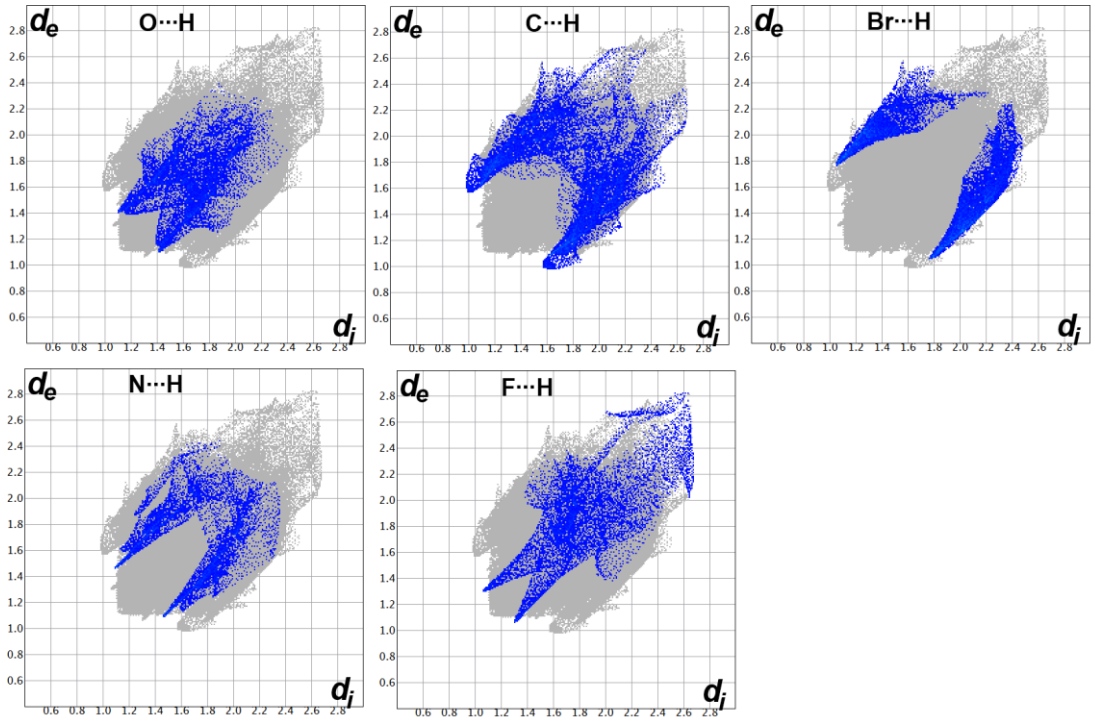

Figure 16. Decomposed fingerprint plots for short contacts in **4i**.

*3.4. MEDT Study of the 32CA Reaction of AY **5b** with Ferrocene Ethylene Derivative **1***

The behaviors of the 32CA reaction of AY **5b** with ferrocene ethylene **1** were studied within MEDT [43] (see Scheme 2).

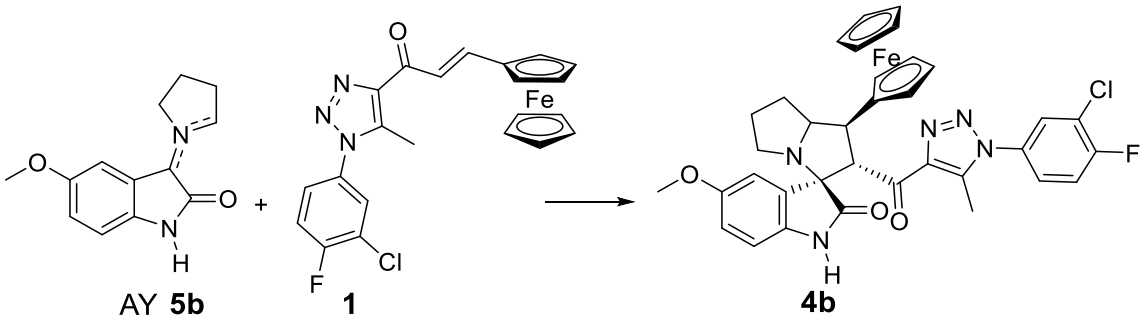

Scheme 2. Studied 32CA reactions of AY **5b** with ferrocene ethylene **1**.

3.4.1. Conceptual DFT Analysis at the Ground State of the Reagents

Analysis of the CDFT reactivity indices [50,51] at the ground state of the reagents is a powerful tool for understanding the reactivity of polar processes [61]. The global reactivity indices, namely, the electronic chemical potential μ, chemical hardness η, electrophilicity ω and nucleophilicity N indices of AY **5b** and ferrocene ethylene **1** are gathered in Table 4.

Table 4. B3LYP/6-31G(d) electronic chemical potential μ, chemical hardness η, electrophilicity ω and nucleophilicity N indices, in eV, of AY **5b** and ferrocene ethylene **1**.

	μ	η	ω	N
ferrocene ethylene **1**	−3.65	3.55	1.87	3.70
AY **5b**	−2.61	3.20	1.07	4.91

The electronic chemical potential [62] of AY **5b**, $\mu = -2.61$ eV, is above that of ferrocene ethylene **1**, $\mu = -3.65$ eV, showing that along a polar 32CA reaction, the GEDT [47] will flux from AY **5b** to the ferrocene ethylene **1**, in a reaction of forward electron density flux (FEDF) [63].

AY **5b** has an electrophilicity ω index [64] of 1.07 eV and a nucleophilicity *N* index [65] of 4.91 eV. Consequently, AY **5b** is classified as a moderate electrophile and a strong nucleophile within the electrophilicity and electrophilicity scales [51]. The very strong nucleophilic character of AY **5b**, higher than 4.0 eV, classifies it as a supernucleophile [51]. On the other hand, ferrocene ethylene **1** has an electrophilicity ω index of 1.87 eV and a nucleophilicity *N* index of 3.70 eV; thus, it is classified as a strong electrophile and strong nucleophile. The supernucleophilic character of AY **5b** and the strong electrophilic character of ferrocene ethylene **1** point out the high polar character of this 32CA reaction of FEDF [63].

3.4.2. Study of the Reaction Mechanism of the 32CA Reaction of AY 5b with Ferrocene Ethylene 1

Exploration of the *ortho*/*endo* reaction path of this 32CA reaction shows that it proceeds via a one-step mechanism (see Scheme 3). Relative electronic energies, in the gas phase and in methanol, of the stationary points involved in this 32CA reaction, are given in Scheme 3. The total electronic energies are given in Table S2 in the Supplementary Materials.

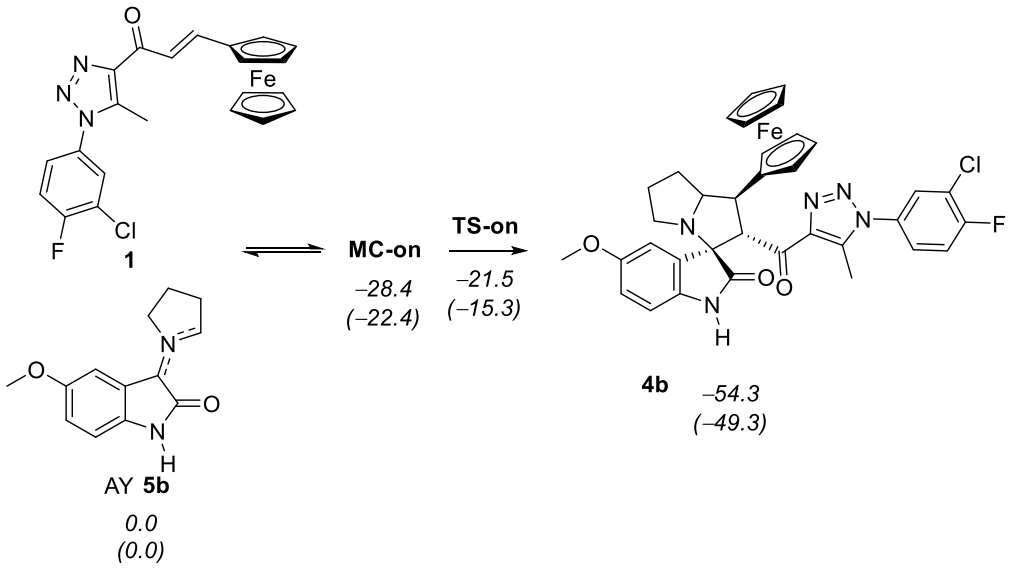

Scheme 3. 32CA reaction of AY **5b** with ferrocene ethylene **1**. Relative electronic energies, with respect to separated reagents, are indicated in italics in kcal·mol^{-1}. ωB97X-D/6-311G(d,p) relative energies in methanol are given in parenthesis.

An exploration of the potential energy surface allows the characterizing of a molecular complex, **MC-on**, in the initial stage of the reaction. **MC-on**, which opens the *ortho*/*endo* reaction path, is positioned 28.4 kcal·mol^{-1} below the separated reagents. **TS-on** is 21.5 kcal·mol^{-1} more stable than the separated reagents. The gas phase activation energy of this 32CA reaction with respect to **MC-on** is positive by 6.8 kcal·mol^{-1}. This reaction is strongly exothermic by −54.3 kcal·mol^{-1}.

The solvent effects of methanol decrease the gas phase relative energies of all species participating in this 32CA reaction by between 5.1 and 6.2 kcal mol^{-1} due to better solvation of the reagents than the other species (see Table S2 in Supplementary Materials). As a consequence, in methanol, the activation energy increases slightly to 7.1 kcal mol^{-1}.

A representation of the enthalpy and Gibbs free-energy profiles associated with the 32CA reaction of AY **5b** with ferrocene ethylene **1** is given in Figure 17. The total and relative enthalpies, entropies and Gibbs free energies are given in Table S3 in the Supplementary Materials. Adding the thermal corrections to the electronic energies in methanol reduces

the relative enthalpies by between 1.0 and 3.4 kcal·mol^{-1}. The relative Gibbs free energies are computed to be between 18 and 22 kcal·mol^{-1} above the enthalpies as a consequence of the unfavorable activation entropies associated with this bimolecular process, which vary between −54 and −64 cal·mol^{-1}·K^{-1}. From **MC-on**, the activation Gibbs free energy associated with this 32CA reaction via **TS-on** increases to 9.2 kcal·mol^{-1}; the formation of **4a** is exergonic by −26.1 kcal·mol^{-1}. It is interesting to highlight that the formation of **MC-on** remains exergonic by −5.0 kcal·mol^{-1}; note that in many 32CA reactions, the formation of this MC is exothermic but endergonic as a consequence of the unfavorable entropic factor associated with their formation.

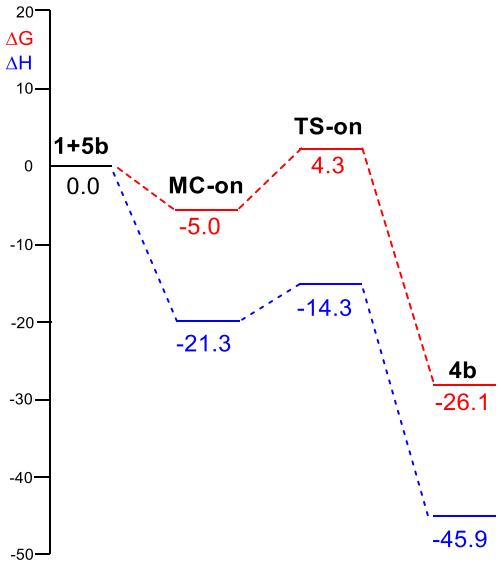

Figure 17. Profiles of MPWB1K/6-311G(d,p) enthalpy (in blue), ΔH in kcal·mol^{-1}, and Gibbs free energy (in red), ΔG in kcal·mol^{-1}, in methanol 1 M at 65 °C, for the 32CA reaction of AY **5b** with ferrocene ethylene **1**.

The geometries of **MC-on** and **TS-on** are given in Figure 18. At **MC-on**, the two interacting species, which show a parallel disposition, are separated by a distance of ca 3.1 Å. At **TS-on**, the distances between the two pairs of interacting carbons, 2.130 and 2.730 Å, show that it is associated with a highly asynchronous C–C single bond formation process resulting from the two-center interaction between the C4 carbon of ferrocene ethylene **1**, and the C3 carbon of AY **5b**. This behavior points out that this 32CA reaction proceeds via a non-concerted *two-stage one-step* mechanism [66] in which the formation of the second C1–C5 single bond begins when the first C3–C4 single bond is practically formed. The solvent effects of methanol do not produce any remarkable change in the gas phase geometries (see Figure 18).

Finally, the analysis of GEDT [47] at **TS-on** allows characterizing the polar character of this 32CA reaction. GEDT values lower than 0.05 e correspond to non-polar processes, while values higher than 0.20 e correspond to high polar processes. The high GEDT value computed at **TS-on**, 0.25 e, is a consequence of the supernucleophilic character of AY **5b** and the strong nucleophilic character of ferrocene ethylene **1**. The flux of the electron density, which goes from AY **5b** to ferrocene ethylene **1**, classifies this 32CA reaction as FEDF, as previously characterized by the CDFT indices. This high GEDT, which favors the bonding changes along the reaction [67], explains that **TS-on** is placed below the separated reagents for enthalpy (see Figure 17).

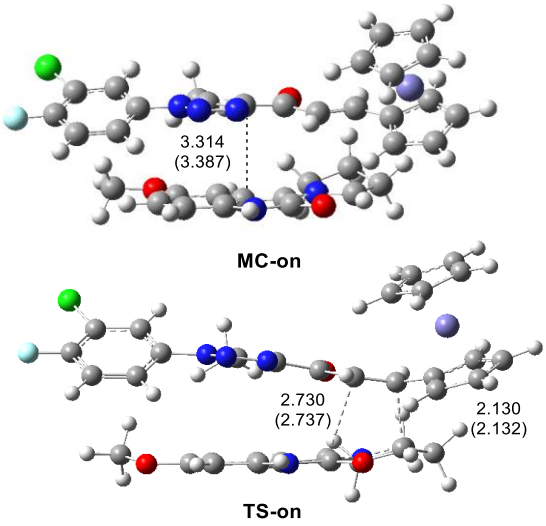

Figure 18. ωB97X-D/6-311G(d,p) geometries of **MC-on** and **TS-on**. The distances are given in Angstrom. Distances in methanol are given in parenthesis.

4. Conclusions

In conclusion, we have successfully synthesized a new set of spiroxindole analogs having a triazole unit with a ferrocene scaffold via the 32CA approach. The 32CA reaction between AY **5b** and ferrocene ethylene **1** has been studied within MEDT. This 32CA reaction proceeds via a non-concerted *two-stage one-step* mechanism involving a highly asynchronous **TS-on**, resulting from the nucleophilic attack of AY **5b** on the β-conjugated position of ferrocene ethylene **1**. The supernucleophilic character of AY **5b,** together with the strong electrophilic character of ferrocene ethylene **1** explain that **TS-on** will be located below reagents. The high GEDT found at **TS-on** accounts for the high polar character of this 32CA reaction of FEDT. Single crystals of the synthesized compounds **4b, 4e, 4h** and **4i** were isolated and examined using X-ray diffraction. The reported structures were found to agree with our synthetic strategy very well. Further, the supramolecular structures of **4b, 4h** and **4i** were described on the basis of Hirshfeld analysis. For **4b,** the O···H, N···H, C···H and H···H contacts are the most important. On the other hand, for **4h**, the H···H, O···H, N···H, C···H, F···H, F···F and Cl···N contacts are the most important, while for **4i,** the O···H, N···H, C···H, Br···H and F···H contacts are the most important. All three compounds showed different extents of π-π stacking interactions.

Supplementary Materials: The following supporting information can be downloaded at: https://www.mdpi.com/article/10.3390/sym14102071/s1. General remarks and X-ray structure determination technical protocol; Tables S1–S3: computational investigations; **Figure S1**. The C-H···N and C-H···O contacts (upper) and the corresponding packing scheme (lower) in **4b**; **Figure S2**. The d_{norm} (left), fingerprint plot (middle) and shape index (right) of π-π stacking interactions in **4i**. Figures S3–S16: Selected NMR (^{1}H and ^{13}C) spectrum of the synthesized compounds.

Author Contributions: Conceptualization, A.B.; methodology, H.H.A.-R., A.M.A.-M. and M.A.; software, M.H., S.M.S., L.R.D. and S.R.; validation, S.M.S., A.E.-F. and L.R.D.; formal analysis, H.H.A.-R., M.A. and S.R.; investigation, H.H.A.-R., A.M.A.-M. and M.A.; resources, A.B.; data curation, M.H., S.M.S., L.R.D. and S.R.; writing—original draft preparation, All authors; writing—review and editing, A.E.-F., S.M.S., L.R.D. and A.B.; supervision, A.B.; funding acquisition, A.B. All authors have read and agreed to the published version of the manuscript.

Funding: The authors would like to extend their sincere appreciation to the Researchers Supporting Project (RSP-2021/64), King Saud University, Riyadh, Saudi Arabia, and the Ministerio de Ciencias, Innovación y Universidades of the Spanish Government, project PID2019-110776GB-I00 (AEI/FEDER, UE).

Institutional Review Board Statement: Not applicable.

Informed Consent Statement: Not applicable.

Data Availability Statement: The data presented in this study are not available on request from the corresponding author.

Acknowledgments: The authors would like to extend their sincere appreciation to the Researchers Supporting Project (RSP-2021/64), King Saud University, Riyadh, Saudi Arabia, and the Ministerio de Ciencias, Innovación y Universidades of the Spanish Government, project PID2019-110776GB-I00 (AEI/FEDER, UE).

Conflicts of Interest: The authors declare no conflict of interest.

References

1. Cerulli, V.; Banfi, L.; Basso, A.; Rocca, V.; Riva, R. Diversity oriented and chemoenzymatic synthesis of densely functionalized pyrrolidines through a highly diastereoselective Ugimulticomponent reaction. *Org. Biomol. Chem.* **2012**, *10*, 1255–1274. [CrossRef] [PubMed]
2. Ganem, B. Strategies for innovation in multicomponent reaction design. *Acc. Chem. Res.* **2009**, *42*, 463–472. [CrossRef] [PubMed]
3. Domling, A. Recent developments in isocyanide based multicomponent reactions in applied chemistry. *Chem. Rev.* **2006**, *106*, 17–89. [CrossRef]
4. Trost, B.M.; Brennan, M.K. Asymmetric Syntheses of Oxindole and Indole Spirocyclic Alkaloid Natural Products. *Synthesis* **2009**, *2009*, 3003–3025. [CrossRef]
5. Jossang, A.; Jossang, P.; Hadi, H.A.; Sevenet, T.; Bodo, B. Horsfiline, an oxindole alkaloid from Horsfieldia superba. *J. Org. Chem.* **1991**, *56*, 6527–6530. [CrossRef]
6. Cui, C.B.; Kakeya, H.; Osada, H. Novel mammalian cell cycle inhibitors, spirotryprostatins A and B, produced by Aspergillus fumigatus, which inhibit mammalian cell cycle at G2/M phase. *Tetrahedron* **1996**, *52*, 12651–12666. [CrossRef]
7. Prado, E.G.; Gimenez, M.D.G.; Vazquez, R.D.L.P.; Sanchez, J.L.E.; Rodriguez, M.T.S. Antiproliferative effects of mitraphylline, a pentacyclic oxindole alkaloid of Uncaria tomentosa on human glioma and neuroblastoma cell lines. *Phytomedicine* **2007**, *14*, 280–287. [CrossRef] [PubMed]
8. Al-Majid, A.M.; Ali, M.; Islam, M.S.; Alshahrani, S.; Alamary, A.S.; Yousuf, S.; Choudhary, M.I.; Barakat, A. Stereoselective Synthesis of the Di-Spirooxindole Analogs Based Oxindole and Cyclohexanone Moieties as Potential Anticancer Agents. *Molecules* **2021**, *26*, 6305. [CrossRef] [PubMed]
9. Barakat, A.; Islam, M.S.; Ali, M.; Al-Majid, A.M.; Alshahrani, S.; Alamary, A.S.; Yousuf, S.; Choudhary, M.I. Regio- and Stereoselective Synthesis of a New Series of Spirooxindole Pyrrolidine Grafted Thiochromene Scaffolds as Potential Anticancer Agents. *Symmetry* **2021**, *13*, 1426. [CrossRef]
10. Kornet, M.J.; Thio, A.P. Oxindole-3-spiropyrrolidines and piperidines. Synthesis and local anesthetic activity. *J. Med. Chem.* **1976**, *19*, 892–898. [CrossRef]
11. Rajanarendar, E.; Ramakrishna, S.; Reddy, K.G.; Nagaraju, D.; Reddy, Y.N. A facile synthesis, anti-inflammatory and analgesic activity of isoxazolyl-2,3- dihydrospiro[benzo[f]isoindole-1,30-indoline]-20,4,9-triones. *Bioorg. Med. Chem. Lett.* **2013**, *23*, 3954–3958. [CrossRef]
12. Rajesh, M.; Perumal, S.; Menéndez, J.C.; Yogeeswari, P.; Sriram, D. Antimycobacterial activity of spirooxindolo-pyrrolidine, pyrrolizine and pyrrolothiazole hybrids obtained by a three-component regio- and stereoselective 1,3-dipolar cycloaddition. *Med. Chem. Commun.* **2011**, *2*, 626–630. [CrossRef]
13. Bhaskar, G.; Arun, Y.; Balachandran, C.; Saikumar, C.; Perumal, P.T. Synthesis of novel spirooxindole derivatives by one pot multicomponent reaction and their antimicrobial activity. *Eur. J. Med. Chem.* **2012**, *51*, 79–91. [CrossRef] [PubMed]
14. Altowyan, M.S.; Barakat, A.; Al-Majid, A.M.; Al-Ghulikah, H.A. Spiroindolone Analogues as Potential Hypoglycemic with Dual Inhibitory Activity on α-Amylase and α-Glucosidase. *Molecules* **2019**, *24*, 2342. [CrossRef] [PubMed]
15. Zhou, W.H.; Xu, X.G.; Li, J.; Min, X.; Yao, J.Z.; Dong, G.Q.; Zhuang, C.L.; Miao, Z.Y.; Zhang, W.N. Design, synthesis and structure–activity relationship of 4, 5-dihydropyrrolo [3, 4-c] pyrazol-6 (1H)-ones as potent p53-MDM2 inhibitors. *Chin. Chem. Lett.* **2017**, *28*, 422–425. [CrossRef]
16. Barakat, A.; Alshahrani, S.; Al-Majid, A.M.; Alamary, A.S.; Haukka, M.; Abu-Serie, M.M.; Dömling, A.; Mazyed, E.A.; Badria, F.A.; El-Senduny, F.F. Novel spirooxindole based benzimidazole scaffold: In vitro, nanoformulation and in vivo studies on anticancer and antimetastatic activity of breast adenocarcinoma. *Bioorg. Chem.* **2022**, *129*, 106124. [CrossRef]
17. Arumugam, N.; Almansour, A.I.; Kumar, R.S.; Dege, N. A facile ionic liquid-accelerated, four-component cascade reaction protocol for the regioselective synthesis of biologically interesting ferrocene engrafted spiropyrrolidine hybrid heterocycles. *J. King Saud Univ. Sci.* **2020**, *32*, 2500–2504. [CrossRef]
18. Zhou, L.-M.; Qu, R.-Y.; Yang, G.-F. An overview of spirooxindole as a promising scaffold for novel drug discovery. *Expert Opin. Drug Discov.* **2020**, *15*, 603–625. [CrossRef]
19. Barakat, A.; Alshahrani, S.; Al-Majid, A.M.; Ali, M.; Altowyan, M.S.; Islam, M.S.; Alamary, A.S.; Ashraf, S.; Ul-Haq, Z. Synthesis of a new class of spirooxindole–benzo[*b*]thiophene-based molecules as acetylcholinesterase inhibitors. *Molecules* **2020**, *25*, 4671. [CrossRef]

20. Lotfy, G.; Aziz, Y.M.A.; Said, M.M.; El Ashry, E.S.H.; El Tamany, E.S.H.; Abu-Serie, M.M.; Teleb, M.; Dömling, A.; Barakat, A. Molecular hybridization design and synthesis of novel spirooxindole-based MDM2 inhibitors endowed with BCL2 signaling attenuation; a step towards the next generation p53 activators. *Bioorg. Chem.* **2021**, *117*, 105427. [CrossRef]
21. Astruc, D. Why is Ferrocene so Exceptional? *Eur. J. Inorg. Chem.* **2017**, *1*, 6–29. [CrossRef]
22. Gasser, G.; Metzler-Nolte, N. The potential of organometallic complexes in medicinal chemistry. *Curr. Opin. Chem. Biol.* **2012**, *16*, 84–91. [CrossRef]
23. Santos, M.M.; Bastos, P.; Catela, I.; Zalewska, K.; Branco, L.C. Recent advances of metallocenes for medicinal chemistry. *Mini-Rev. Med. Chem.* **2017**, *17*, 771–784. [CrossRef]
24. Top, S.; Vessières, A.; Leclercq, G.; Quivy, J.; Tang, J.; Vaissermann, J.; Huché, M.; Jaouen, G. Synthesis, biochemical properties and molecular modelling studies of organometallic specific estrogen receptor modulators (SERMs), the ferrocifens and hydroxyferrocifens: Evidence for an antiproliferative effect of hydroxyferrocifens on both hormone-dependent and hormone-independent breast cancer cell lines. *Chem. A Eur. J.* **2003**, *9*, 5223–5236.
25. Dubar, F.; Khalife, J.; Brocard, J.; Dive, D.; Biot, C. Ferroquine, an ingenious antimalarial drug-thoughts on the mechanism of action. *Molecules* **2008**, *13*, 2900–2907. [CrossRef]
26. Ferreira, V.F.; da Rocha, D.R.; da Silva, F.C.; Ferreira, P.G.; Boechat, N.A.; Magalhães, J.L. Novel 1 H-1, 2, 3-, 2 H-1, 2, 3-, 1 H-1, 2, 4-and 4 H-1, 2, 4-triazole derivatives: A patent review (2008–2011). *Expert Opin. Ther. Pat.* **2013**, *23*, 319–331. [CrossRef]
27. Salmon, A.J.; Williams, M.L.; Wu, Q.K.; Morizzi, J.; Gregg, D.; Charman, S.A.; Vullo, D.; Supuran, C.T.; Poulsen, S.A. Metallocene-based inhibitors of cancerassociated carbonic anhydrase enzymes IX and XII. *J. Med. Chem.* **2012**, *55*, 5506–5517. [CrossRef] [PubMed]
28. Kumar, K.; Carrere-Kremer, S.; Kremer, L.; Guerardel, Y.; Biot, C.; Kumar, V. 1 H-1, 2, 3-triazole-tethered isatineferrocene and isatineferrocenylchalcone conjugates: Synthesis and in vitro antitubercular evaluation. *Organometallics* **2013**, *32*, 5713–5719. [CrossRef]
29. Kumar, K.; Carrère-Kremer, S.; Kremer, L.; Guérardel, Y.; Biot, C.; Kumar, V. Azide–alkyne cycloaddition en route towards 1 H-1, 2, 3-triazole-tethered β-lactam–ferrocene and β-lactam–ferrocenylchalcone conjugates: Synthesis and in vitro anti-tubercular evaluation. *Dalton Trans.* **2013**, *42*, 1492–1500. [CrossRef]
30. Kumar, K.; Pradines, B.; Madamet, M.; Amalvict, R.; Benoit, N.; Kumar, V. 1H-1, 2, 3-triazole tethered isatin-ferrocene conjugates: Synthesis and in vitro antimalarial evaluation. *Eur. J. Med. Chem.* **2014**, *87*, 801–804. [CrossRef] [PubMed]
31. Van Staveren, D.R.; Metzler-Nolte, N. Bioorganometallic chemistry of ferrocene. *Chem. Rev.* **2004**, *104*, 5931–5986. [CrossRef] [PubMed]
32. Xu, J.; Yang, Y.; Baigude, H.; Zhao, H. New ferrocene–triazole derivatives for multisignaling detection of Cu^{2+} in aqueous medium and their antibacterial activity. *Spectrochim. Acta Part A Mol. Biomol. Spectrosc.* **2020**, *229*, 117880. [CrossRef] [PubMed]
33. Arivazhagan, C.; Borthakur, R.; Ghosh, S. Ferrocene and triazole-appended rhodamine based multisignaling sensors for Hg2+ and their application in live cell imaging. *Organometallics* **2015**, *34*, 1147–1155. [CrossRef]
34. Fouda, M.F.; Abd-Elzaher, M.M.; Abdelsamaia, R.A.; Labib, A.A. On the medicinal chemistry of ferrocene. *Appl. Organomet. Chem.* **2007**, *21*, 613–625. [CrossRef]
35. Larik, F.A.; Saeed, A.; Fattah, T.A.; Muqadar, U.; Channar, P.A. Recent advances in the synthesis, biological activities and various applications of ferrocene derivatives. *Appl. Organomet. Chem.* **2017**, *31*, e3664. [CrossRef]
36. Domingo, L.R.; Ríos-Gutiérrez, M.; Barakat, A. A molecular electron density theory study of the [3+2] cycloaddition reaction of an azomethine ylide with an electrophilic ethylene linked to triazole and ferrocene units. *Molecules* **2022**, *27*, 6532. [CrossRef] [PubMed]
37. Haque, A.; Hsieh, M.F.; Hassan, S.I.; Faizi, M.S.H.; Saha, A.; Dege, N.; Rather, J.A.; Khan, M.S. Synthesis, characterization, and pharmacological studies of ferrocene-1H-1, 2, 3-triazole hybrids. *J. Mol. Struct.* **2017**, *1146*, 536–545. [CrossRef]
38. Ríos-Gutiérrez, M.; Barakat, A.; Domingo, L.R. A Molecular Electron Density Theory Study of the [3 + 2] Cycloaddition Reaction of *Pseudo(mono)radical* Azomethine Ylides with Phenyl Vinyl Sulphone. *Organics* **2022**, *3*, 122–136. [CrossRef]
39. Barakat, A.; Haukka, M.; Soliman, S.M.; Ali, M.; Al-Majid, A.M.; El-Faham, A.; Domingo, L.R. Straightforward regio- and diastereoselective synthesis, molecular structure, intermolecular interactions and mechanistic study of spirooxindole-engrafted rhodanine analogs. *Molecules* **2021**, *26*, 7276. [CrossRef]
40. Altowyan, M.S.; Soliman, S.M.; Haukka, M.; Al-Shaalan, N.H.; Alkharboush, A.A.; Barakat, A. Synthesis and Structure Elucidation of Novel Spirooxindole Linked to Ferrocene and Triazole Systems via [3 + 2] Cycloaddition Reaction. *Molecules* **2022**, *27*, 4095. [CrossRef] [PubMed]
41. Chai, J.-D.; Head-Gordon, M. Long-range corrected hybrid density functionals with damped atom–atom dispersion corrections. *Phys. Chem. Chem. Phys.* **2008**, *10*, 6615–6620. [CrossRef] [PubMed]
42. Hehre, M.J.; Radom, L.; Schleyer, P.V.R.; Pople, J. *Ab Initio Molecular Orbital Theory*; Wiley: New York, NY, USA, 1986.
43. Domingo, L.R. Molecular electron density theory: A modern view of reactivity in organic chemistry. *Molecules* **2016**, *21*, 1319. [CrossRef] [PubMed]
44. Tomasi, J.; Persico, M. Molecular interactions in solution: And overview of methods based on continuous distributions of the solvent. *Chem. Rev.* **1994**, *94*, 2027–2094. [CrossRef]
45. Simkin, B.Y.; Sheikhet, I.I. *Quantum Chemical and Statistical Theory of Solutions—Computational Approach*; Ellis Horwood: London, UK, 1995.

46. Marenich, A.V.; Cramer, C.J.; Truhlar, D.G. Universal Solvation Model Based on Solute Electron Density and on a Continuum Model of the Solvent Defined by the Bulk Dielectric Constant and Atomic Surface Tensions. *J. Phys. Chem. B* **2009**, *113*, 6378–6396. [CrossRef] [PubMed]
47. Domingo, L.R. A new C–C bond formation model based on the quantum chemical topology of electron density. *RSC Adv.* **2014**, *4*, 32415–32428. [CrossRef]
48. Reed, A.E.; Weinstock, R.B.; Weinhold, F. Natural population analysis. *J. Chem. Phys.* **1985**, *83*, 735–746. [CrossRef]
49. Reed, A.E.; Curtiss, L.A.; Weinhold, F. Intermolecular interactions from a natural bond orbital, donor-acceptor viewpoint. *Chem. Rev.* **1988**, *88*, 899–926. [CrossRef]
50. Parr, R.G.; Yang, W. *Density Functional Theory of Atoms and Molecules*; Oxford University Press: Oxford, UK, 1989.
51. Domingo, L.R.; Ríos-Gutiérrez, M.; Pérez, P. Applications of the conceptual density functional indices to organic chemistry reactivity. *Molecules* **2016**, *21*, 748. [CrossRef]
52. Frisch, M.J.; Trucks, G.W.; Schlegel, H.B.; Scuseria, G.E.; Robb, M.A.; Cheeseman, J.R.; Scalmani, G.; Barone, V.; Petersson, G.A.; Nakatsuji, H.; et al. (Eds.) *Gaussian 16, Revision A.03*; Gaussian, Inc.: Wallingford, CT, USA, 2016.
53. Otwinowski, Z.; Minor, W. Processing of X-ray Diffraction Data Collected in Oscillation Mode. In *Methods in Enzymology, Macromolecular Crystallography, Part A*; Carter, C.W., Sweet, J., Eds.; Academic Press: New York, NY, USA, 1997; Volume 276, pp. 307–326.
54. Rikagu Oxford Diffraction. *CrysAlisPro*; Rikagu Oxford Diffraction Inc.: Oxfordshire, UK, 2022.
55. Sheldrick, G.M. *SADABS—Bruker Nonius Scaling and Absorption Correction*; Bruker AXS, Inc.: Madison, WI, USA, 2012.
56. Sheldrick, G.M. SHELXT-Integrated Space-Group and Crystal-Structure Determination. *Acta Crystallogr. Sect. A Found. Adv.* **2015**, *71*, 3–8. [CrossRef] [PubMed]
57. Sheldrick, G.M. Crystal Structure Refinement with SHELXL. *Acta Crystallogr. Sect. C Struct. Chem.* **2015**, *71*, 3–8. [CrossRef]
58. Hübschle, C.B.; Sheldrick, G.M.; Dittrich, B. *ShelXle*: A Qt graphical user interface for *SHELXL*. *J. Appl. Crystallogr.* **2011**, *44*, 1281–1284. [CrossRef] [PubMed]
59. Spek, A.L. PLATON SQUEEZE: A tool for the calculation of the disordered solvent contribution to the calculated structure factors. *Acta Crystallogr. Sect. C Struct. Chem.* **2015**, *C71*, 148–155.
60. Turner, M.J.; McKinnon, J.J.; Wolff, S.K.; Grimwood, D.J.; Spackman, P.R.; Jayatilaka, D.; Spackman, M.A. *Crystal Explorer17*; University of Western Australia: Crawley, WA, Australia, 2017; Available online: http://hirshfeldsurface.net (accessed on 20 July 2020).
61. Domingo, L.R.; Ríos-Gutiérrez, M. *Application of Reactivity Indices in the Study of Polar Diels–Alder Reactions, in Conceptual Density Functional Theory: Towards a New Chemical Reactivity Theory*; Liu, S., Ed.; Wiley-VCH GmbH: Weinheim, Germany, 2022; Volume 2, pp. 481–502.
62. Parr, R.G.; Pearson, R.G. Absolute hardness: Companion parameter to absolute electronegativity. *J. Am. Chem. Soc.* **1983**, *105*, 7512–7516. [CrossRef]
63. Domingo, L.R.; Ríos-Gutiérrez, M.; Pérez, P. A Molecular Electron Density Theory Study of the Reactivity of Tetrazines in Aza-Diels-Alder Reactions. *RSC Adv.* **2020**, *10*, 15394–15405. [CrossRef]
64. Parr, R.G.; Szentpaly, L.V.; Liu, S. Electrophilicity index. *J. Am. Chem. Soc.* **1999**, *121*, 1922–1924. [CrossRef]
65. Domingo, L.R.; Chamorro, E.; Pérez, P. Understanding the reactivity of captodative ethylenes in polar cycloaddition reactions. A theoretical study. *J. Org. Chem.* **2008**, *73*, 4615–4624. [CrossRef]
66. Domingo, L.R.; Sáez, J.A.; Zaragozá, R.J.; Arnó, M. Understanding the Participation; f Quadricyclane as Nucleophile in Polar [2 sigma+2 sigma+2 pi] Cycloadditions toward Electrophilic pi Molecules. *J. Org. Chem.* **2008**, *73*, 8791–8799. [CrossRef]
67. Domingo, L.R.; Ríos-Gutiérrez, M.; Pérez, P. How does the global electron density transfer diminish activation energies in polar cycloaddition reactions? A Molecular Electron Density Theory study. *Tetrahedron* **2017**, *73*, 1718–1724. [CrossRef]